# Transposable Element-Mediated Epigenomic Remodeling Drives Erythropoietin-Induced Neurogenesis in the Adult Hippocampus

Umut Cakir[1,2], Melanie Fritz[3], Umer Javed Butt[1,3], Riki Kawaguchi[4], Daniel Geschwind[4,5], Klaus-Armin Nave[6], Hannelore Ehrenreich[# 1,2,3] and Manvendra Singh[# 1,3]

[1]*Clinical Neuroscience, Max Planck Institute for Multidisciplinary Sciences, City Campus, Göttingen, Germany*

[2]*Georg-August-University, Göttingen, Germany*

[3]*Experimental Medicine, Department of Psychiatry and Psychotherapy, Central Institute of Mental Health, Medical Faculty Mannheim, Heidelberg University, J 5, Mannheim, Germany*

[4]*Center for Neurobehavioral Genetics, Semel Institute for Neuroscience and Human Behavior, University of California Los Angeles, Los Angeles, CA, USA*

[5]*Institute of Precision Health, University of California Los Angeles, Los Angeles, CA, USA*

[6]*Department of Neurogenetics, Max Planck Institute for Multidisciplinary Sciences, City Campus, Göttingen, Germany*

[#] Corresponding authors

**Running Head: Erythropoietin and transposable elements**

**Key Words: EPO, TE, therapy, cognitive and neuropsychiatric disorders**

**# Correspondence:**

**Dr. Manvendra Singh, PhD**
Department of Psychiatry and Psychotherapy,
Central Institute of Mental Health,
Medical Faculty Mannheim, Heidelberg University, J 5,
68159 Mannheim, Germany
Phone: +49 (176) 670 23344
E-mail: manvendra.singh@mpinat.mpg.de

**Prof. Hannelore Ehrenreich, MD, DVM**
Experimental Medicine, Department of Psychiatry and Psychotherapy
Central Institute of Mental Health
Medical Faculty Mannheim, Heidelberg University, J 5,
68159 Mannheim, Germany
Phone: +49-160-97000331
E-Mail: hannelore.ehrenreich@zi-mannheim.de

## ABSTRACT

Understanding the molecular mechanisms by which erythropoietin (EPO) is associated with neurogenesis is essential to harness its therapeutic potential for cognitive and neuropsychiatric disorders. Here, we employed single-nucleus assay for transposase-accessible chromatin sequencing (snATAC-seq), combined with single-nucleus RNA sequencing (snRNA-seq), to map the epigenomic and transcriptional landscapes of adult mouse hippocampus under recombinant human EPO (rhEPO) treatment. We discovered significant lineage-specific remodelling of chromatin accessibility predominantly in newly formed pyramidal neurons, highlighting a robust EPO-driven neurogenic response. Notably, transposable elements (TEs), particularly ancient LINEs and SINEs, emerged as critical cis-regulatory elements extensively bound by key neurogenic transcription factors such as NEUROD1/2, FOXG1, and ASCL1. Integrative analyses revealed that these TE-derived regulatory elements orchestrate gene networks involved in neuronal differentiation, synaptogenesis, and synaptic plasticity. Our findings highlight a previously unrecognised role of TEs as dynamic regulators in EPO-induced hippocampal re-wiring of gene regulatory networks associated with neurogenesis, establishing a valuable epigenomic resource for advancing therapeutic strategies targeting cognitive deficits and neurodegenerative conditions.

## INTRODUCTION

Erythropoietin (EPO) is the hypoxia-inducible glycoprotein growth hormone classically known for its essential role in driving erythropoiesis[1]. Beyond this hematopoietic function, EPO is also expressed by a trove of cell types within the adult brain, especially in the hippocampus, where it functions as a pleiotropic neurotrophic factor that is postulated to promote neuroplasticity, support neuronal survival, and induce synaptic remodelling[2]. In consequence, EPO produced in the central nervous system has key beneficial roles in neuroprotection and cognitive function[3]. Evidently, administration of recombinant human EPO (rhEPO) has been shown to alleviate cognitive deficits in clinical trials involving patients with neuropsychiatric disorders and brain injuries[4], and also conferred neuroprotection in neurodegenerative models[2,5]. At the molecular level, several neuronal and glial lineages endogenously express EPO and its canonical receptor (EPOR)[6], establishing an endogenous neuro-EPO system during intense cognitive or motor activity.

The hippocampus is an extraordinarily heterogeneous structure, composed of diverse neuronal and glial lineages whose contributions to neurogenesis and cognition are governed by cell-type-specific regulatory networks. Bulk genomics lacks the resolution to pinpoint such cell-restricted changes, whereas single-cell approaches now overcome this hurdle. Recent single-cell transcriptomic studies revealed that recombinant human EPO (rhEPO) re-wires hippocampal networks, promoting pyramidal neuron differentiation and synaptogenesis, while reducing inhibitory interneurons[7,8]. Electrophysiology confirmed that these newly integrated CA1 neurons receive stronger excitatory and weaker inhibitory input. In parallel, EPO induces plasticity-associated genes and chromatin regulators, including *BDNF*, *GAP43*, *PSD95*, *EGR1*, and *EP300*, and functionally exports *HDAC5*, pointing to deeper epigenomic remodelling[3,7,9]. This prompted us to perform single-nucleus ATAC-seq (snATAC-seq), which maps chromatin accessibility at single-cell resolution and identifies candidate cis-regulatory elements (cCREs: proximal promoters and distal enhancer-promoter sequences) that control cell-type-specific gene expression programs[10]. The snATAC-seq on hippocampi of mice treated with rhEPO allows us to capture dynamic regulatory events in rare hippocampal subpopulations and define the cCREs engaged by EPO, providing critical insights into how it reprograms neurogenic gene expression[7,11,12].

An emerging insight from epigenomic studies is that transposable elements (TEs) constitute a significant and previously underappreciated source of cCREs in the brain[13]. These repetitive elements make up a large fraction of the mammalian genome (half of human and mouse genome), are frequently co-opted as cCREs controlling the neighboring gene expression[13–16]. In

fact, a substantial subset of brain-specific cCREs is derived from TEs. For instance, in the human cortex, around 80% of recently gained (human-specific) regulatory elements overlap TEs[17]. Notably, species-specific endogenous retrovirus (ERV),SINE transposons, and even the DNA transposons have been shown to serve as cCREs in neural progenitors, providing novel binding sites for neurogenic transcription factors (TFs)[18,19]. Given their abundance and regulatory malleability, TE-derived sequences represent a compelling, yet unexplored, component of the hippocampal regulatory genome that might mediate stimulus-driven transcriptional responses. However, it remains unclear whether adult neurogenesis is induced by external stimuli such as EPO, and if so, then whether it harnesses these TE-derived regulatory sequences to drive gene expression programs in newly formed neurons. We therefore hypothesised that pro-neurogenic effects of rhEPO could involve remodelling of these TE-derived cCREs in specific hippocampal cell types.

Here, leveraging high-resolution snATAC-seq in combination with snRNA-seq and TF chromatin immunoprecipitation sequencing (ChIP-seq), we present a comprehensive atlas of chromatin accessibility in the adult mouse hippocampus following rhEPO treatment. Our integrative analyses reveal that rhEPO profoundly remodels the epigenomic landscape, selectively enhancing chromatin accessibility at TE-derived regulatory elements mainly within excitatory, that too particularly in newly formed neurons, highlighting TEs as facilitators of adaptive gene regulatory responses in the mammalian brain. Finally, we show these TE-derived differentially accessible regions (DARs) are co-bound by canonical neurogenic transcription factors (e.g., NEUROD1/2, ASCL1, SOX2, PAX6) and link to nearby genes involved in neuronal differentiation and synaptic integration, which display coordinated accessibility and expression gains in pyramidal and dentate-gyrus lineages. These findings pin a new epigenetic dimension to EPO's cognitive-enhancing effects, including TE-driven regulatory networks that orchestrate neuronal plasticity and synaptic integration. In summary, this work points towards the neurotrophic action of EPO from gene expression changes to the level of chromatin regulation, revealing a previously unrecognised TE-driven mechanism that facilitates adult neurogenesis and circuit remodelling in the EPO-treated brain.

# RESULTS

## Single-cell chromatin accessibility profiling uncovers the 35 cell clusters residing in the adult mouse hippocampus

We performed snATAC-seq on the right hippocampus of eight adult mice (four rhEPO-treated, four placebo-treated), using a modified protocol based on previous snATAC-seq methods[20,21]. Sequencing generated 9.16×10^8 paired-end reads, from which ~35,000 high-quality nuclei passed stringent filtering. Standard snATAC QC metrics were robust: we observed strong transcription-start-site (TSS) enrichment and characteristic nucleosomal banding, with <5% of fragments mapping to ENCODE blacklist regions. Data processing utilized the Signac framework[22] for peak calling and matrix generation, followed by batch correction via Harmony[23] (Fig. 1A). We next performed dimensionality reduction by latent semantic indexing (LSI) and uniform manifold approximation (UMAP) to visualize the data (Fig. 1B). Unsupervised clustering resolved 35 distinct accessibility-defined clusters, which were annotated into 11 major hippocampal lineages: Dentate gyrus, excitatory (pyramidal) and inhibitory neurons, microglia, astrocytes, oligodendrocytes,, endothelial cells, pericytes, intermediate, ependymal, and neuroimmune cells (Fig. 1B-C). Annotation was guided by accessibility at canonical marker loci: for example, astrocyte clusters showed prominent accessibility at the *Slc1a2* locus, whereas dentate gyrus neuron clusters were marked by *Prox1* peaks[20], and neuronal clusters by pan-neuronal loci (*Slc17a7 as in vGlut2*) while oligodendrocyte-lineage clusters featured Plp1/*Mbp*/*Mog* or *Pdgfra* accessibility, etc (Fig. 1G). These chromatin-defined identities aligned with our matched snRNA-seq data from the left hippocampus of the same animals: cross-modal label transfer yielded highly concordant cell-type assignments (Fig. 1C-E, Fisher's Exact Test; p-value < 0.05), confirming the accuracy of our annotations. Together, this integrated multi-omic atlas delineates the cell-type-specific regulatory landscape of the adult hippocampus, linking candidate cis-regulatory elements to gene expression programs. In this line, distribution of peaks across hippocampal lineages further highlights distinct cis-regulatory signatures for each cell type (Fig. 1F). These integrated multi-omic analyses provide a foundation for constructing gene regulatory networks underlying hippocampal cell identity and the effects of rhEPO treatment. For instance, we observed that the *Slc1a2* (*EAAT2*) promoter is broadly accessible across multiple hippocampal lineages, whereas its distal enhancers are selectively open in astrocytes, yielding astrocyte-specific expression (Fig. 1G). This fits the established principle that promoters are often ubiquitously accessible while enhancer deployment is cell-type specific,

as shown by ENCODE-scale promoter cCRE analyses[24] and by astrocyte maturation studies documenting enhancer accessibility remodelling[25].

## Characterization of hippocampal regulatory regions

To infer regulatory programs monitoring the identity of hippocampal lineages, we examined TF motif enrichment in the cluster-specific accessible regions. We found 135 unique TF motifs significantly enriched (log2 enrichment ratio > 2 and adjusted p-value < $1e^{-10}$) across the 35 hippocampal clusters and their representative 11 lineages, emphasizing an unusually broad regulatory diversity (Fig. 2A). Among the enriched motifs were those of well-known neurogenic regulators: for example, SOX TFs[26] , members of the EGR family[27], the NEUROD1/2 and NEUROG1/2 factors, essential for neuronal differentiation[28,29] and NRF1, a metabolic regulator that activates neuronal and synaptic genes under activity[30]. Notably, we also uncovered motifs for TFs not previously emphasized in hippocampal biology: for example, GLIS1/2, ZBTB14, RFX2/5, the NR4A2::RXRA heterodimer, ZNF423, a zinc-finger TF implicated in neurodevelopment[31]. These motif enrichments showed lineage-specific patterns: OLIG-like and SOX-family motifs were predominant in glial clusters, consistent with oligodendrocyte/astrocyte programs[32], whereas EGR/ERG motifs dominated progenitor and early neuronal clusters except the interneurons, reflecting excitability-dependent genes and cell-cycle control in neural precursors[27,33]. In contrast, ETS/ELF motifs were highly enriched in endothelial and microglial clusters, aligning with their known association with immune regulatory programs[34] (Fig. 2A). Together, the breadth and coherence of these motif signatures reinforce the robustness of our cell-type annotations and markedly expand the known transcriptional regulatory landscape of the adult hippocampus.

## Transposable elements contribute substantially to the cis-regulatory architecture of the adult hippocampus

To further characterize cCREs across hippocampal cell types, we classified aggregated snATAC-seq peaks by genomic context. Overlaying peak summits with mm10 gene models revealed that only 10.4% of accessible regions overlapped annotated promoter regions (±1 kb of transcription start sites), while 44.5% localized within introns, 36.9% in intergenic regions, and 4.3% within annotated gene bodies (exons and UTRs) (Fig. 2B). Comparison with the recent single-cell atlas of the adult mouse brain[35] revealed that ~10.8% of our hippocampal peaks were absent from prior annotations, indicating a set of unreported, potentially hippocampus-specific cCREs (Fig. 2B). Given that intergenic and intronic regions harbor the bulk of enhancers, we

next focused on TEs, which constitute roughly half of the mammalian genome[16] and are increasingly recognized as a major source of regulatory innovation. TEs frequently carry inducible enhancer or promoter activities, especially in the brain, where they have been shown to re-wire gene regulatory networks during development and evolution[18,36,37]. Using chromatin accessibility at TE insertions, we found that ~20% of hippocampal cCREs overlapped annotated TEs (including LTRs, LINEs, SINEs, etc.), consistent with previous reports that ~25% of mammalian cCREs are TE-derived[36] (Fig. 2C). Notably, LTR elements exhibited disproportionately high accessibility, consistent with the view that LTRs often function as self-contained regulatory modules for neighbor gene expression[36,37] (Fig. 2D). Among these, subfamilies such as ERVK, ERVL, RMER1A, RMER1B, IAPEY4, LTR41 and ORR1E showed the most significant enrichment in cCRE repertoires (Fig. 2D-E). These TE-derived cCREs may serve as lineage-specific regulatory elements influencing hippocampal gene programs, for example, those underlying synaptic plasticity, neurogenesis or memory consolidation[38,39]. Together, these findings reveal that TEs are extensively integrated into the adult hippocampal regulatory network, providing a pool of fresh, cell type enriched cCREs that likely contribute to hippocampal function.

## Epigenomic remodeling and enriched neuroplasticity regulators under rhEPO

To capture the global effects of rhEPO on hippocampal chromatin accessibility, we analyzed ATAC-seq peaks that differed significantly between EPO- and placebo-treated samples, independent of cell-type identity. Comparing the overall data, we identified 976 DARs between the rhEPO and placebo conditions, comprising 816 regions of gained chromatin accessibility and 160 regions of accessibility loss in EPO-treated hippocampi (Fig. 3A). Upon mapping the proximity of these DARs from the annotated TSS in the genome, we found that 639 of them were located within ±1 kb from TSS of known genes, out of which a substantial fraction of them overlapped with TE sequences (Fig. 3B). We then subjected these 639 genes to a gene ontology analysis, which indicated that these DAR-associated genes are significantly enriched in pathways for neuroplasticity, synapse organisation, and cognitive function, indicating a plausible mechanism of how EPO might re-wire the neurogenesis-associated transcriptional networks (Fig. 3C). For instance, we detected robust EPO-induced chromatin accessibility at the promoters of nearest gained Ascl1 - transcriptional regulators that promote neural progenitor differentiation [40,41]. Likewise, Egr2, an immediate-early gene of the EGR family implicated in neuronal plasticity[42] (Fig. 3A). This finding is further supported by TF binding motif enrichment analysis of these DARs, which revealed a convergence on TF families that govern neurogenesis

and synaptic plasticity (Fig. 3D). Specifically, rhEPO-open chromatin regions were highly enriched for binding motifs of Kruppel-like factors (KLF), which is consistent with KLFs established role in neuronal maturation and associated with adult neurogenesis[43] as well as early growth response factors (EGR1–3), which are immediate-early TFs critical for learning and memory[42,44,45]. Notably, motifs for AP-2 (TFAP2) factors, which modulate adult glutamatergic neurogenesis[46], and GLIS factors were over-represented. Additionally, rhEPO-responsive sites were enriched for ETS-family motifs (including ELK1/ELF2), which are downstream effectors of ERK/MAPK signaling in neurons and mediate activity-dependent gene induction[47]. Elements recognized by CREB/ATF family members (e.g. Atf1) were likewise enriched, fitting with the known role of CREB/ATF factors as positive regulators of memory consolidation[48]. Together, these results indicate that rhEPO treatment engages a broad network of neuronal gene regulators that collectively drive excitatory neuron differentiation and synaptic growth.

Importantly, upon overlaying the similar analysis of differentially expressed genes (DEGs) from our snRNA-seq data, we observed a strong correlation between DARs identified by snATAC-seq and DEGs from our parallel snRNA-seq analysis, particularly for DARs proximal to DEGs (Fig. 3E). This correlation indicates that chromatin remodeling mediated by rhEPO precedes and are functionally concordant with transcriptional changes in hippocampal lineages. Our parallel snRNA-seq dataset too shows higher expression of Egr2, Syt4, Nrg3, Nrp1 and many other DAR-associated genes in EPO-treated hippocampus than in controls (Fig. 3E)[7,8]. Several synaptic genes exhibited enhanced accessibility only in EPO-treated nuclei, such as Synaptotagmin-4 (Syt4), an activity-inducible vesicle protein that modulates BDNF release and learning-related synaptic plasticity, and Neuregulin-3 (Nrg3), a trophic factor that promotes excitatory synapse formation on interneurons[49,50]. We also found differential peaks at the Neuropilin-1 (Nrp1) locus, a receptor for axonal guidance cues (semaphorins). Thus, rhEPO application not only activates these pro-neurogenic and plasticity-related genes at the chromatin level, but also overexpresses their transcription, suggesting a coordinated epigenome-transcriptome response underlying EPO-induced alterations in the neural network.

Intriguingly, a significant fraction of the EPO–placebo differences in chromatin accessibility maps to TEs within the genome. We found that roughly 50% of EPO-gained DARs overlap TEs, predominantly rodent-specific SINEs of the B1/Alu and B2 families (including subtypes such as *ID_B1*, *B3*, *B1_Mus1/2*) (Fig. 3B and 3F). These observations suggest that EPO-driven regulatory changes may, in part, co-opt TE sequences as enhancers or promoter modules in the adult brain. This is in line with emerging evidence that SINE-derived DNA and transcripts can serve normal neuronal functions[51]. More generally, SINE retrotransposons can recruit

transcriptional regulators or RNA-binding proteins to nearby genes, thereby modulating gene expression in cis[51,52]. Next, we compared EPO-induced accessibility at TE-derived DARs with differential expression of their nearest genes and observed a robust concordance, whereby gains in accessibility tended to accompany gene upregulation. The enrichment of B1/B2 SINE elements within EPO-responsive chromatin regions, in a close vicinity of DEG genes (Fig. 3F) implies that the retrotransposon sequences may be tapped to mediate the far-reaching gene program activated by EPO.

## Lineage-Specific Chromatin Remodeling and TE-Driven GRN Activation in the Adult Mouse Hippocampus by EPO

To determine whether rhEPO exerts equal or lineage-specific effects on hippocampal chromatin states, we assessed differential chromatin accessibility across each of the 11 major hippocampal lineages provided in[7] from the same set of mice. Using the logistic regression (LR) test with adjusted $P < 0.01$ threshold, we identified a total of 39404 genome-wide DARs in all 11 lineages taken together. Although a subset of these DARs (n = 7,608) was common to multiple lineages, the majority (n = 21,555) were lineage-specific (Fig. 4A). While cataloguing the DARs in individual lineage, we found remarkably that pyramidal neurons alone accounted for approximately 50% (~22,000) of the total DARs, highlighting their pronounced chromatin responsiveness to rhEPO treatment (Fig. 4B). To assess the differential promoter activity, we tested what fraction of DARs in each of 11 lineages falls within 1 kb range of the TSS of annotated genes. We found a myriad of promoter accessibility across hippocampal lineages, as coinciding with the total DAR distribution pattern around the TE sequences and TSS of known genes. Interestingly, the distribution pattern of DARs among TEs and TSS between the 11 lineages was consistently proportional. Pyramidal neurons exhibited by far the greatest number of DARs on TE sequences (n = 3,897) and on the promoters of genes (n=1849), with an inclined bias toward increased chromatin accessibility, as 1065 TSS were upregulated versus 784 downregulated regions (Fig. 4B).

Dentate gyrus showed the next highest DAR count (n = 6,131) but an opposite trend, as a majority of these regions had depleted accessibility for TEs (455 up vs. 726 down) and gene-TSSs (291 up vs. 305 down), whereas glial populations, oligodendrocytes (742 DARs), astrocytes (581 DARs) and Microglia (308 DARs) displayed moderate numbers of EPO-responsive TSSs, skewed slightly toward openness. Whereas interneurons (347 DARs) exhibited the reverse pattern, with predominantly downregulated regions (159 up versus 188 down). Endothelial, Pericytes, neuroimmune, intermediate and ependymal cells were least

affected (Fig. 4B). Thus, the majority of DARs in pyramidal neurons, microglia, and oligodendrocytes were upregulated, whereas dentate gyrus cells and interneurons showed predominantly downregulated DARs. Overall, this distribution pattern suggests that EPO's chromatin remodelling effects are directed primarily toward excitatory lineage expansion and glial physiology, while concurrently limiting the accessibility changes associated with inhibitory neuronal programs.

We next tested a model, based on the above observations, in which EPO promotes open chromatin in excitatory neurons and glial cells by investigating if the key neurogenic gene promoters are significantly upregulated in rhEPO samples. Expectedly, pyramidal neurons showed the activation of key neurogenic TFs and developmental regulators. For instance, Ascl1, Neurog2, and Pax6, the key factors driving neuronal commitment from precursors[53,54], and Nrg3, a neuregulin promoting excitatory synaptogenesis[50], all exhibited robust accessibility gains in pyramidal neurons, dentate gyrus, astrocytes, and oligodendrocytes (Fig. 4C). In addition to these established neurogenic genes, several less-characterised but pertinent regulators emerged among the top EPO-responsive promoters. For instance, the zinc-finger factors *Zbtb16* (Plzf) and *Zbtb18* (Rp58), both implicated in cortical neurogenesis and neuronal subtype development[55,56], showed increased accessibility, as did *Fabp5*, *Mdga2*, and *Dusp6* (Fig. 4C). The enrichment of these diverse gene promoters suggests that EPO activates a broad pro-neurogenic chromatin landscape, encompassing classical neurogenesis drivers and novel regulatory elements linked to neuronal maturation, migration, and synaptic integration.

Given these findings, we hypothesized that rhEPO treatment might differentially re-wire GRNs in hippocampal pyramidal and glial lineages. To systematically test this hypothesis, we applied the Pando algorithm, integrating our matched snRNA-seq and snATAC-seq datasets, to identify key TFs, their target regulatory regions, and downstream effector genes[57]. This analysis revealed that although most regulons were conserved between rhEPO and placebo conditions, we identified approximately a dozen regulons displaying specific enrichment under rhEPO (Fig. 4D). Notably, these rhEPO-enriched regulons were prominently driven by TFs involved in neuronal differentiation and maturation (Fig. 4D). These observations support the model that rhEPO specifically engages neurogenic TFs to facilitate the activation of genes essential for neuronal development and synaptic plasticity.

Additionally, we also found that a broad spectrum of TE families was significantly enriched within the DARs (Fig. 4E). These enriched repeats included LTR retrotransposons of the ORR1E and MTD families, ancient LINEs L2/L2a and SINEs rodent B families B3, B4/B4A, the mammalian-wide interspersed repeat MIR/MIRb, which is an evolutionarily old SINE family[58–60].

This widespread TE activation is consistent with prior evidence that such elements can be co-opted as cCREs in neural cells[61–63]. Among many evidence of TE-derived cCREs, we observe L2c, MER103C/MIR, and B1_Mur4 being upregulated in rhEPO samples and seem to provide regulatory sequences to the TSS of Phf24, Cpne5, and Haus6 genes, respectively (Fig. 4F). These patterns indicate that EPO treatment broadly unlocks repeat-rich genomic regions in a lineage-specific manner, suggestive of TE families enriched in EPO-induced DARs that can act as regulatory DNA elements that influence gene transcription.

## Lineage-specific chromatin remodeling predominantly affects pyramidal neurons

We had shown that in rhEPO-treated mice, excitatory neuron line, particularly CA1 pyramidal cells were markedly over-represented, while the proportion of GABAergic interneurons was reduced[7,8]. Notably, we observed a dramatic expansion of newly formed pyramidal neuron subpopulations, with up to a fivefold increase (~500% of control levels) in rhEPO samples. These findings extend prior single-cell analyses showing ~2-fold enrichment (~200%) of immature pyramidal neurons after EPO and are consistent with earlier reports that prolonged EPO treatment increases mature CA1 pyramidal neuron numbers by ~20%[7,12]. Even a single EPO dose is known to acutely elevate immature glutamatergic precursors within hours[12]. To further delineate how EPO orchestrates transcriptional networks underlying neurogenesis, we performed high-resolution chromatin accessibility clustering of pyramidal neuron lineages from our snATAC-seq data. Initial clustering from snRNA-seq identified 20 distinct pyramidal clusters[7], whereas snATAC-seq revealed 29 distinct clusters. Cross-modal integration allowed us to robustly annotate these clusters into 17 distinct cell types, showing substantial concordance between snRNA-seq and snATAC-seq modalities (Fig. 5A). The two predominant pyramidal subgroups were newly formed (early-stage markers) and mature neurons (late-stage markers) that exhibited complete congruence between modalities, clearly segregating into discrete UMAP clusters. Following these leads, we next sought to characterize chromatin accessibility differences between newly formed and mature pyramidal neurons, specifically evaluating the contribution of TE-derived cCREs. Differential accessibility analysis identified 7,420 DARs distinguishing these two populations, of which 1,705 DARs mapped within gene promoters and 935 overlapped TE sequences (Fig. 5B). Remarkably, ~66 % of promoter-associated DARs displayed significantly higher chromatin accessibility in newly formed neurons, with gene ontology analyses revealing significant enrichment for neurogenesis and synaptic formation (Fig. 5C). Of note, we observed that around 83% of promoter and TE-associated DARs were upregulated in rhEPO samples.

We further investigated chromatin accessibility differences between rhEPO and placebo conditions within immature versus mature pyramidal neurons. Consistent with expectations, mature pyramidal neurons exhibited limited chromatin remodeling (~7,000 DARs) compared to newly formed neurons (~11,000 DARs) with ~65% upregulated and ~35% downregulated in the both cases (Fig. 5E). These results suggest the diminished epigenetic plasticity potential of rhEPO upon neuronal maturation. Within newly formed neurons, alongside a plenty of promoter-proximal DARs (n=946, ±1 kb from TSS), we identified an additional ~4,000 distal DARs (within ±10 kb of gene TSS), marking putative enhancers and distal cCREs responsive to rhEPO (Fig. 5F). These distal regions prominently featured immediate-early genes (Egr1, Egr2, Egr3), known mediators of neuronal activation and synaptic plasticity, as well as key neuronal specification genes (Ascl1, Bcl11a, Nrg3), and epigenetic regulators (Dnmt3a, Setd5) (Fig. 5G). Collectively, these data suggest that rhEPO preferentially promotes broad epigenomic remodeling and neurogenic transcriptional programs in newly formed neurons, while inducing limited, targeted adjustments in mature neurons.

## TE-Linked Neurogenic Enhancer Activity on EPO-Induced Chromatin Remodeling

We subsequently examined whether the DARs induced by rhEPO overlapping TEs participate specifically in GRNs activated in newly formed neurons. In newly formed (immature) pyramidal neurons, we identified a substantially greater number of EPO-induced TE-derived differentially accessible regions (TE-DARs) compared to mature pyramidal neurons, at both promoter-proximal and distal genomic locations. Interestingly, mature neurons showed merely 1253, whereas newly formed neurons featured 1,934 TE-DARs, with 844 located within a range of ±10 kb near gene promoters (Fig. 6A). To further investigate the regulatory context of these sites, we intersected the TE-DARs with ChIP-seq profiles for 12 neurogenic transcription factors (TFs) (FOXG1, PAX6, ASCL1, NEUROG1/2, NEUROD1/2, SOX2, TBR1, EGR1, FOXO3, FOS, and JUN). Using established permutation tests[64], we found hundreds of TE-DARs bound by one or more of these TFs - far more than expected by chance (Fig. 6B and Fig. 7A-C). Among TFs, NEUROD1 and FOXG1 exhibited the most extensive binding across TE families (295 and 256 TE families, respectively (pval < 0.001). A core set of 24 TE families, including ancient LINEs (L2, L3), LTR retrotransposons (LTR33, MER130, MLT1 series), and SINE elements (AmnSINE1, MamSINE1), was commonly enriched across multiple neurogenic TFs (Fig. 6C). Notably, many of these TE families have previously been exapted as gene regulatory enhancers in the brain. For instance, MER130 elements harbor consensus NEUROD/NEUROG-binding motifs and have been shown to function as enhancers during mouse neocortical development[65].

Likewise, AmnSINE1, an ancient SINE family, has well-documented enhancer activity crucial for mammalian brain development[66]. Together, our findings indicate that TE insertions from specific families have been specifically co-opted as part of the cis-regulatory repertoire of neurogenic TFs in mammalian brain.

To explore the functional relevance of these TE-derived DARs bound by neurogenic TFs, we examined the genes located nearby. We found 42 TE-containing DARs (filtered by >10% cells expressing at least in one condition) within 10 kb of range from genes TSS. Consistent with our thesis, gene ontology analysis showed that the nearest genes to TF-bound TE-DARs were highly enriched for biological processes related to neurogenesis and synaptic integration. Notably, genes nearest to these TE-DARs have well-documented roles in neuronal differentiation and synapse development, such as Hes5, Kcnma1, Pacsin1, Ankef1, Rab4a, Nptxr, and Nedd4l (Fig. 6D-E). These results demonstrate that ancient TE sequences serve as regulatory elements specifically during the developmental window of new neuron formation, thus enhancing expression of genes critical for neuronal integration and synaptic plasticity. Furthermore, chromatin accessibility at these TF-bound TE-DARs was markedly increased in rhEPO samples (FDR < 0.01), which was accompanied by concordant transcriptional upregulation of nearby genes specifically in newly formed neurons and dentate gyrus (Fig. 6E). For instance, our selected aforementioned candidates were exclusively accessible in rhEPO newly formed neurons, potentially driving the expression of several genes, as these genes are upregulated in our snRNA-seq data (Fig. 6E-F). In summary, our findings underscore an innovative regulatory mechanism whereby rhEPO engages TE-derived enhancers via neurogenic TFs, facilitating epigenomic reprogramming essential for hippocampal neurogenesis and synaptic plasticity.

## DISCUSSION

In this study, we constructed a high-resolution atlas of chromatin accessibility in the adult mouse hippocampus and demonstrated that EPO, a traditionally hematopoietic hormone, can profoundly reprogram the adult neural epigenome to drive neurogenesis. This expands upon prior single-cell brain atlases[10,67] by focusing on the hippocampus and incorporating an experimental perturbation (EPO), thereby providing new insights into how adult neurogenic niches can be modulated. Crucially, we found that EPO's effects are highly cell-type-specific,

predominantly impacting excitatory neuron lineages (pyramidal neurons), which showed the most pronounced chromatin remodeling and population expansion in response to treatment.

## EPO as a potent extrinsic modulator of adult hippocampal neurogenesis

These findings enrich our understanding of adult hippocampal neurogenesis, a process first recognized in rodents in the 1960s[68,69] and later confirmed in humans using classical and current state-of-the-art methods[70,71]. The adult hippocampus retains progenitor cells that can differentiate into new neurons mainly in response to intrinsic or extrinsic stimuli. While we lack the temporal data, our results position EPO as a potential extrinsic trigger of hippocampal neurogenesis, consistent with earlier observations that EPO improves cognitive function and enhances neuroplasticity[2,12,72]. *In vivo* studies in healthy mice and clinical trials in patients have shown that EPO can improve learning and memory independent of its role in erythropoiesis[2,73–75]. We recently reported that EPO treatment increases mature pyramidal neuron numbers by ~20% and newly formed neurons by ~200% without altering cell proliferation, suggesting EPO promotes differentiation or maturation of pre-existing neural precursors. In this study, we observed a substantially greater relative expansion (~5-fold) of the young pyramidal neuron population under EPO. This striking difference may either reflect the sensitivity of our chromatin-based approach in capturing nascent neurons, as well as a possibly more robust EPO regimen, or a region biasness in some samples. These hypothesis still remains to be tested. Importantly, our data support the model that EPO drives the differentiation of progenitors rather than inducing widespread cell division, as we detected increased accessibility at neurogenic transcription factor loci (e.g., *Ascl1*, *Neurog2*, *Nrg3 etc.,*) but did not observe evidence of aberrant cell-cycle activation in non-neuronal lineages. This aligns with the notion that EPO biases cell fate choice toward neurons in the existing precursor pool. The net effect is an enrichment of pyramidal neurons at the cost of interneurons. Pyramidal neurons integrate in the hippocampal circuitry, leading to potential implications for mood, memory, cognitive enhancement and recovery from brain injury.

### TEs as a regulatory innovation in hippocampal gene regulation

Despite TE known roles in other brain regions, the contribution of TEs to regulatory landscapes in the adult hippocampus has remained unexplored at single-cell resolution. One of the major highlights from our study is the extent to which TEs contribute to the gene regulatory changes underlying the EPO-induced phenomenon in hippocampi. We found that roughly one-fifth of all open chromatin regions in the adult hippocampus are derived from TEs, even under basal conditions. This observation is in line with large-scale epigenomic surveys showing that a

substantial fraction of brain-specific cis-regulatory elements are TE-derived[35]. Notably, the hippocampus, particularly the dentate gyrus, a hub of adult neurogenesis, has been reported to exhibit high levels of TE activity and mosaicism[71]. TEs are thought to create genomic variability in neural progenitors and even generate long non-coding RNAs in the brain that fine-tune gene expression[62,76]. Our results extend these findings by pinpointing specific TE families that function as accessible chromatin sites in distinct hippocampal cell types. For example, we observed that certain LINE, SINE, and endogenous retrovirus (ERV) families such as RMER1 retrotransposons and IAPEY4/ORR1 endogenous retroviral elements are enriched in open chromatin unique to hippocampal neurons. These TE-derived sequences appear to serve as cell-type-specific enhancers or promoters, an interpretation supported by their overlap with known neuronal gene loci and motif enrichments.

TEs are increasingly recognized as drivers of gene regulatory network evolution. Many TEs carry binding site motifs for transcription factors and can thereby introduce novel regulatory modules. Classic examples include the co-option of a SINE element (*AmnSINE1*) as an enhancer essential for mammalian brain development[51,52] and the MER130 DNA transposon family, providing binding sites for neural transcription factors in the developing cortex[62,63]. Our data demonstrate that similar TE-mediated regulatory mechanisms are active in the adult hippocampus. We found motifs for neural fate determinants e.g., NeuroD**,** Sox, Klf embedded within several TE sequences that are accessible in neurogenic cell clusters. EPO's influence on the epigenome appears to leverage this TE repertoire. Remarkably, by aggregating all hippocampus cells, we observed that about 50% of the regions that gained DARs with EPO treatment were endogenous retroelement-derived sequences (Fig. 3) which is a proportion far exceeding their baseline representation. This enrichment suggests that EPO may activate a specific subclass of dormant regulatory elements to drive the nearby genes. One intriguing possibility is that these TE-DARs carry latent binding motifs for inducible transcription factors and become functional enhancers only under certain stimuli, as in this case, EPO stimulation. Such a mechanism would represent a previously unappreciated mode of gene regulation: the *de novo* recruitment of ancient genomic elements to drive a contemporary cellular response.

## Mechanisms of EPO-mediated neuroplasticity

Our integrative multi-omic analysis sheds light on the gene regulatory networks fine-tuned by EPO and how they intersect with TEs. By combining chromatin accessibility data with matched single-cell transcriptomes and leveraging a network inference algorithm, we identified key EPO-responsive regulons which are sets of transcription factors and target genes that act in

cascades. Prominently featured in these regulons were classical neurogenic transcription factors like NEUROD1**,** NEUROD2**,** FOXG1**,** PAX6**,** and JUN**,** known to orchestrate the progression of neural stem cells into mature neurons[77]. In EPO-treated hippocampi, these factors were not only upregulated at the mRNA level in pyramidal lineages, but their binding motifs were also significantly enriched in the EPO-gained accessible chromatin regions, and many of those were derived from TEs. This implies that EPO induces a feed-forward loop: it elevates neurogenic TF expression, and those TFs in turn bind to and activate TE-derived cCREs associated with neuron-specific genes, reinforcing the neurogenic program. Our incorporation of external ChIP-seq data from developing brain or neural culture systems provided orthogonal validation for this model, showing, for example, that NEUROD1/2 and NEUROG2 binding sites overlap many of the LINE/SINE/ERV-derived cCREs that EPO opened *in vivo*. While these findings resonate with reports that cell-type-specific TFs often exploit transposon-derived sequences for binding[78], here we demonstrate this phenomenon in an active, inducible context within the adult brain.

Taken together, we propose a conserved evolutionary mechanism at play: ancient TEs embedded in the genome have been repurposed as cCREs in neural cells, and during an EPO-induced neurogenic stimulus, the brain taps into this reservoir of regulatory elements to rapidly reshape gene expression. In evolutionary terms, this represents an efficient strategy – rather than evolving entirely new gene regulatory sequences from scratch, genome has preserved a large bank of TE-derived cCREs that lie dormant until the appropriate transcriptional signals such as those triggered by EPO/EPOR signaling, activate them. The outcome is a robust transcriptional activation of neurogenesis-promoting genes. This concept aligns with the hypothesis that TEs facilitate the acquisition of novel cis-regulatory elements over evolutionary time[37,79], and our data illustrate that such TE-facilitated regulatory innovation can be deployed within a single organism's lifespan, enabling context-specific gene regulation to adapt to physiological stimuli.

**Implications of EPO-mediated re-wiring of GRNs in regenerative therapy**

Our study carries broad implications. First, it highlights a previously underappreciated molecular pathway by which extrinsic factors like EPO can induce neuroplastic changes: through large-scale epigenomic remodeling of chromatin accessibility. This complements classical signaling and gene expression analyses by demonstrating that changes in the "accessibility" of the genome are a critical intermediate step linking external signals to sustained cellular phenotypes. Of note, EPO is known to be upregulated in the brain under hypoxic or injury conditions, and it has been considered a natural neuroprotective agent[75,80]. Our findings raise the possibility that

part of the brain's injury response may involve EPO-driven engagement of transposon-based cCREs to activate genes for repair, regeneration, or circuit reorganization. Second, our work highlights the functional importance of the vast repetitive genome in normal physiology. Whereas TEs have traditionally been studied in the context of genome instability or evolution, here we show they play a central role in acute, beneficial plasticity of the adult brain when challenged by external stimuli. This bridges the gap between transposon biology and neurobiology, suggesting that they are intimately involved in processes like learning, memory, and regeneration. Finally, from a translational perspective, identifying TE-derived cCREs that are activated by pro-neurogenic stimuli could open new therapeutic strategies. If certain transposon-derived cCREs are master switches for neurogenic gene programs, they might be targeted by gene editing or epigenetic drugs to stimulate neuron replacement in aging or neurological disorders. Moreover, our single-cell atlas of hippocampal chromatin accessibility, with and without EPO is a valuable resource for the neuroscience community. It provides a catalogue of candidate regulatory elements for each major hippocampal cell type. In summary, our work not only reveals a new biological mechanism by which EPO potentially induces neurogenesis but also lays a foundation for future explorations into the "regulatory dark matter" of the genome in adult brain function and therapy.

**CONCLUSION**

While our study delivering rhEPO-mediated epigenomic reorganization in the adult hippocampus is profound, it also confers obvious limitations. Firstly, our analysis captures a snapshot of a single time point after EPO treatment where we could not resolve the dynamic sequences of chromatin and transcriptional changes. While we identified a strong association between TFs-TEs interplay and chromatin accessibility as a proxy for regulatory activity maneuvered by EPO, the targeted perturbation e.g., CRISPR deletion of a candidate TE enhancer, and other epigenetic layers such as histone modifications or 3D chromatin architecture will be necessary to confirm the causality. Despite these limitations, our work reveals a compelling new paradigm in which an exogenous factor (rhEPO) leverages the genomic potential of transposable elements to execute a complex biological program (neurogenesis). This insight expands our understanding of gene regulation in the adult brain and could inform novel strategies to enhance brain repair, cognitive function, and resilience against neurodegenerative conditions. By uncovering the latent regulatory power of transposons in neural plasticity, we pave the way for future studies to explore the therapeutic modulation of the "repeatome" in the service of regenerative medicine.

## METHODS

### Ethical approval

All animal experiments were approved by the local Animal Care and Use Committee (Niedersächsisches Landesamt für Verbraucherschutz und Lebensmittelsicherheit, LAVES) and conducted in strict accordance with the German Animal Protection Law.

### Experimental model and treatments

Male C57BL/6N mice received intraperitoneal injections of recombinant human erythropoietin (rhEPO, 5000 IU/kg body weight) or placebo (0.01 mL/g of solvent) every other day for three weeks, starting at postnatal day 28 (P28). For single-cell profiling, 23 male C57BL/6N mice were sacrificed on postnatal day 49 (P49), 24 hours after the final intraperitoneal injection of recombinant human erythropoietin (rhEPO, n = 11) or placebo (n = 12). Mice were euthanized via cervical dislocation, and the hippocampi were rapidly dissected on an ice-cold surface, snap-frozen in liquid nitrogen, and stored at –80 °C until processing. For each sample, two right hippocampi from mice of the same treatment group were pooled into a single tube (except for one rhEPO sample, which included only one hippocampus), resulting in six biological replicates per condition (N = 6 rhEPO, N = 6 placebo) for snRNA-seq (GSE220522). Likewise, the left hippocampi from 4 tubes from each group (N = 4 rhEPO, N = 4 placebo, tube labels are: A1, A2, A4, A6, B7, B8, B9, B11) were used for scATAC-seq. The snATAC-seq library construction is done for these eight hippocampal samples using Chromium Single Cell ATAC Library & Gel Bead Kit v2 chemistry.

### Single-cell ATAC-seq library processing and alignment

snATAC-seq libraries were generated and processed using the Cell Ranger ATAC pipeline (v2.1.0, 10x Genomics). Raw reads from eight hippocampal samples were aligned to the mm10 reference genome (refdata-cellranger-arc-mm10-2020-A-2.0.0). Peak-barcode matrices and fragment files were generated using cellranger-atac count and used for downstream analysis.

### Unified-peak set workflow

Downstream analysis was performed in R using the Signac (v1.13.0) and Seurat (v5.1.0) packages. Individual peak files were merged into a unified peak set using reduce() from the GenomicRanges package, excluding peaks <20 bp or >10,000 bp. Cells with fewer than 500 fragments in peaks were filtered out. Chromatin assays were constructed for each sample using FeatureMatrix().

Each Seurat object was annotated using EnsDb.Mmusculus.v79, and quality control (QC) metrics were computed: transcription start site (TSS) enrichment, nucleosome signal, percent reads in peaks, and blacklist ratio (based on blacklist_mm10). Cells were filtered using quantile-

based thresholds, excluding outliers (below 2nd or above the 98th percentile for key metrics) to remove low-quality cells and potential multiplets.

Filtered objects were merged, then the merged object was processed with normalization with RunTFIDF(), dimensionality reduction via latent semantic indexing (RunSVD()), batch correction with harmony (RunHarmony() using LSI dims 2–30), and UMAP embedding. Clusters were identified with FindNeighbors() and FindClusters() with resolution 0.8 and algorithm 1. Gene activity scores were calculated via GeneActivity() and log-normalized with NormalizeData() (scale factor = median of nCount_Activity). A preprocessed single-nucleus RNA-seq dataset (Singh et al., 2023) served as a reference for cell type annotation. Unmatching samples (A3, A5, B10, B12) were excluded. Anchors were computed using canonical correlation analysis (CCA) to predict cells in scATAC-seq dataset.

**Sample-specific peak set workflow**

In addition to the unified peak set approach, we conducted a complementary analysis using sample-specific peak sets generated by Cell Ranger ATAC. For each sample, peak-barcode matrices and fragment files were independently loaded, and chromatin assays were constructed using a minimum cell threshold of min.cells = 10. Seurat objects were generated separately for each sample and subsequently merged for integrated downstream analysis. Gene annotations were added using the EnsDb.Mmusculus.v79 database. QC metrics were calculated for each cell, including TSS enrichment, nucleosome signal, percent reads in peaks, and the blacklist ratio. To ensure high-quality samples, cells were filtered using the following strict criteria: nCount_peaks between 3,000 and 30,000, pct_reads_in_peaks > 15%, blacklist_ratio < 0.05, nucleosome_signal < 4, and TSS.enrichment > 3.

Dimensionality reduction and clustering were performed: normalization with RunTFIDF(), feature selection via FindTopFeatures(min.cutoff = 'q0'), latent semantic indexing (LSI) using RunSVD() on dimensions 2 through 8, and UMAP embedding via RunUMAP(). Clusters were identified using FindNeighbors() and FindClusters() with algorithm 1. Gene activity scores were computed using GeneActivity() and log-normalized with NormalizeData(). Cell type annotations previously inferred from the unified peak set analysis were transferred to the sample-specific peak set dataset by matching shared cell barcodes. Cells without annotation were excluded from further analysis.

For analysis related to the Pyramidal cluster, pyramidal neurons were subset from the unified peak set dataset and subjected to reclustering to refine subtype resolution. To facilitate annotation, these cells were integrated with a previously annotated single-nucleus RNA-seq reference dataset (Singh et al., 2023) using CCA, with 30 dimensions and 10 nearest neighbors

employed to identify cross-modality anchors. Uncharacterized or ambiguous Seurat clusters were either removed or reannotated based on their transcriptomic profiles and proximity to well-defined clusters in the reference dataset. The finalized annotations were then transferred to the corresponding pyramidal neuron populations within the sample-specific peak set dataset by matching shared cell barcodes.

**Differential Accessibility (DA) Analysis**

All rhEPO- and placebo-derived cells were combined within each cluster (seurat cluster, higher-level cell-type annotation, or pyramidal subclusters). We then executed FindMarkers (test.use = "LR", min.pct = 0.01, latent.vars = "nCount_peaks") in a one-versus-rest fashion to identify peaks that are intrinsically enriched or depleted in a given cluster relative to all other clusters. We used 0.01 as min.pct threshold to capture accessibility shifts in smaller subfractions of a population. Peaks passing FDR < 0.01 were considered cell-type DA peaks. Furthermore, to pinpoint treatment-dependent changes, we stratified cells by condition inside each cluster and ran FindMarkers() with min.pct = 0.01 in the LR framework, and depth correction was applied. Peaks with FDR < 0.01 were classified as condition DA peaks. In differences between defined clusters (cell-type DA peaks) or treatment-dependent changes (condition DA peaks), summits (peak mid-points) were annotated via TxDb.Mmusculus.UCSC.mm10.knownGene to the closest gene's promoter, binned by genomic context (promoter, exon, intron, intergenic) and intersected with RepeatMasker (mm10) to identify and quantify overlap with TEs. Low-complexity, satellite, RNA, rRNA, tRNA, scRNA, snRNA, RC, srpRNA, and ambiguous repeats (entries flagged with "?" such as "LINE?") were excluded from all TE analyses unless explicitly stated.

**Cluster-resolved motif enrichment**

Chromatin dynamics were analyzed in two complementary tiers: chromatin accessibility differences between defined clusters and treatment-dependent changes. Vertebrate position-frequency matrices from the JASPAR-2020 CORE collection were added for motif analysis. For every Seurat cluster, higher-level cell-type annotation, or pyramidal subclusters, identified DA peaks using FindMarkers were filtered as min.pct threshold is 0.10, only positive, and FDR < 0.05. Clusters contributing ≥ 10 significant peaks were subjected to motif enrichment with FindMotifs(). Likewise, within the same clustering framework, cells were split by condition, and DA peaks filtered with min.pct threshold is 0.10, only positive, and FDR < 0.05 parameters were used for motif analysis. For any cluster yielding ≥ 10 rhEPO-responsive peaks, FindMotifs() was run to identify transcription-factor motifs enriched in rhEPO-gained chromatin.

**Transcription-factor ChIP-seq integration**

Genome-wide binding profiles for 13 neurodevelopmental transcription factors (ASCL1, EGR1, FOS, FOXG1, FOXO3, JUN, NEUROD1, NEUROD2, NEUROG2, PAX6, SOX2, TBR1) were downloaded from GEO. Peak files were lifted over to the mm10 assembly where necessary (UCSC liftOver) and collapsed into non-redundant consensus regions with bedtools merge function. To ask whether individual TFs preferentially occupy repeat-derived regulatory DNA, we quantified intersections between each consensus ChIP peak set and RepeatMasker annotations using regioneR; 1000 permutations provided empirical P values and observed/expected overlap ratios. TE-associated peaks were assigned to the nearest transcription-start site with ChIPseeker (TxDb.Mmusculus.UCSC.mm10.knownGene) and subjected to GO-biological-process enrichment with clusterProfiler::enrichGO (BH-adjusted $q \leq 0.01$). Next, TF peaks were overlapped with the 11 broad cell-class DA peak lists and the refined pyramidal-lineage DA peaks identified in our snATAC-seq analysis.

**Data availability**

All raw FASTQ files, fragment files, count matrices, and Seurat objects underlying the present study have been deposited in the GSEXXX and zenodo.XXX.

**Code availability**

Code for data processing, quality control, clustering, differential-accessibility testing, motif analysis, and TF-ChIP overlap is available on the following GitHub link:
https://github.com/umutcakir/ATAC_EPO_vs_Placebo

# References


1. Byts N, Sirén AL. Erythropoietin: a multimodal neuroprotective agent. *Exp Transl Stroke Med*. 2009;1:4. doi:10.1186/2040-7378-1-4

2. Adamcio B, Sargin D, Stradomska A, et al. Erythropoietin enhances hippocampal long-term potentiation and memory. *BMC Biol*. 2008;6(1):37. doi:10.1186/1741-7007-6-37

3. Miskowiak KW, Vinberg M, Christensen EM, et al. Recombinant human erythropoietin for treating treatment-resistant depression: a double-blind, randomized, placebo-controlled phase 2 trial. *Neuropsychopharmacology*. 2014;39(6):1399-1408. doi:10.1038/npp.2013.335

4. Grimm G, Stockenhuber F, Schneeweiss B, Madl C, Zeitlhofer J, Schneider B. Improvement of brain function in hemodialysis patients treated with erythropoietin. *Kidney Int*. 1990;38(3):480-486. doi:10.1038/ki.1990.229

5. Sargin D, El-Kordi A, Agarwal A, et al. Expression of constitutively active erythropoietin receptor in pyramidal neurons of cortex and hippocampus boosts higher cognitive functions in mice. *BMC Biol*. 2011;9:27. doi:10.1186/1741-7007-9-27

6. Ott C, Martens H, Hassouna I, et al. Widespread Expression of Erythropoietin Receptor in Brain and Its Induction by Injury. *Mol Med*. 2015;21(1):803-815. doi:10.2119/molmed.2015.00192

7. Singh M, Zhao Y, Gastaldi VD, et al. Erythropoietin re-wires cognition-associated transcriptional networks. *Nat Commun*. 2023;14(1):4777. doi:10.1038/s41467-023-40332-8

8. Curto Y, Carceller H, Klimczak P, et al. Erythropoietin restrains the inhibitory potential of interneurons in the mouse hippocampus. *Mol Psychiatry*. Published online April 15, 2024. doi:10.1038/s41380-024-02528-2

9. Liu B, Wen JK, Li BH, et al. Celecoxib and acetylbritannilactone interact synergistically to suppress breast cancer cell growth via COX-2-dependent and -independent mechanisms. *Cell Death Dis*. 2011;2(7):e185. doi:10.1038/cddis.2011.64

10. Li YE, Preissl S, Hou X, et al. An atlas of gene regulatory elements in adult mouse cerebrum. *Nature*. 2021;598(7879):129-136. doi:10.1038/s41586-021-03604-1

11. Rey F, Balsari A, Giallongo T, et al. Erythropoietin as a Neuroprotective Molecule: An Overview of Its Therapeutic Potential in Neurodegenerative Diseases. *ASN Neuro*. 2019;11:1759091419871420. doi:10.1177/1759091419871420

12. Wakhloo D, Scharkowski F, Curto Y, et al. Functional hypoxia drives neuroplasticity and neurogenesis via brain erythropoietin. *Nat Commun*. 2020;11(1):1313. doi:10.1038/s41467-020-15041-1

13. Sundaram V, Wysocka J. Transposable elements as a potent source of diverse cis-regulatory sequences in mammalian genomes. *Philos Trans R Soc Lond B Biol Sci*. 2020;375(1795):20190347. doi:10.1098/rstb.2019.0347

14. Jönsson ME, Garza R, Johansson PA, Jakobsson J. Transposable Elements: A Common Feature of Neurodevelopmental and Neurodegenerative Disorders. *Trends Genet*. 2020;36(8):610-623. doi:10.1016/j.tig.2020.05.004

15. Monsen Ø, Grønvold L, Datsomor A, et al. The role of transposon activity in shaping cis-regulatory element evolution after whole-genome duplication. *Genome Res*. 2025;35(3):475-488. doi:10.1101/gr.278931.124

16. Wells JN, Feschotte C. A Field Guide to Eukaryotic Transposable Elements. *Annu Rev Genet*. 2020;54(1):539-561. doi:10.1146/annurev-genet-040620-022145

17. Zemke NR, Armand EJ, Wang W, et al. Conserved and divergent gene regulatory programs of the mammalian neocortex. *Nature*. 2023;624(7991):390-402. doi:10.1038/s41586-023-06819-6

18. Patoori S, Barnada SM, Large C, Murray JI, Trizzino M. Young transposable elements rewired gene regulatory networks in human and chimpanzee hippocampal intermediate progenitors. *Development*. 2022;149(19). doi:10.1242/dev.200413

19. Pulver C, Grun D, Duc J, et al. Statistical learning quantifies transposable element-mediated cis-regulation. *Genome Biol*. 2023;24(1):258. doi:10.1186/s13059-023-03085-7

20. Sinnamon JR, Torkenczy KA, Linhoff MW, et al. The accessible chromatin landscape of the murine hippocampus at single-cell resolution. *Genome Res*. 2019;29(5):857-869. doi:10.1101/gr.243725.118

21. Preissl S, Fang R, Huang H, et al. Single-nucleus analysis of accessible chromatin in developing mouse forebrain reveals cell-type-specific transcriptional regulation. *Nat Neurosci*. 2018;21(3):432-439. doi:10.1038/s41593-018-0079-3

22. Stuart T, Srivastava A, Madad S, Lareau CA, Satija R. Single-cell chromatin state analysis with Signac. *Nat Methods*. 2021;18(11):1333-1341. doi:10.1038/s41592-021-01282-5

23. Korsunsky I, Millard N, Fan J, et al. Fast, sensitive and accurate integration of single-cell data with Harmony. *Nat Methods*. 2019;16(12):1289-1296. doi:10.1038/s41592-019-0619-0

24. Fan K, Moore JE, Zhang XO, Weng Z. Genetic and epigenetic features of promoters with ubiquitous chromatin accessibility support ubiquitous transcription of cell-essential genes. *Nucleic Acids Res*. 2021;49(10):5705-5725. doi:10.1093/nar/gkab345

25. Lattke M, Goldstone R, Ellis JK, et al. Extensive transcriptional and chromatin changes underlie astrocyte maturation in vivo and in culture. *Nat Commun*. 2021;12(1):4335. doi:10.1038/s41467-021-24624-5

26. Favaro R, Valotta M, Ferri ALM, et al. Hippocampal development and neural stem cell maintenance require Sox2-dependent regulation of Shh. *Nat Neurosci*. 2009;12(10):1248-1256. doi:10.1038/nn.2397

27. O'Donovan KJ, Tourtellotte WG, Millbrandt J, Baraban JM. The EGR family of transcription-regulatory factors: progress at the interface of molecular and systems neuroscience. *Trends Neurosci*. 1999;22(4):167-173. doi:10.1016/s0166-2236(98)01343-5

28. Toda T, Parylak SL, Linker SB, Gage FH. The role of adult hippocampal neurogenesis in brain health and disease. *Mol Psychiatry*. 2019;24(1):67-87. doi:10.1038/s41380-018-0036-2

29. Noack F, Vangelisti S, Raffl G, et al. Multimodal profiling of the transcriptional regulatory landscape of the developing mouse cortex identifies Neurog2 as a key epigenome remodeler. *Nat Neurosci*. 2022;25(2):154-167. doi:10.1038/s41593-021-01002-4

30. Cheng A, Wan R, Yang JL, et al. Involvement of PGC-1α in the formation and maintenance of neuronal dendritic spines. *Nat Commun*. 2012;3:1250. doi:10.1038/ncomms2238

31. Deshpande O, Lara RZ, Zhang OR, Concepcion D, Hamilton BA. ZNF423 patient variants, truncations, and in-frame deletions in mice define an allele-dependent range of midline brain abnormalities. *PLoS Genet*. 2020;16(9):e1009017. doi:10.1371/journal.pgen.1009017

32. Zhou Q, Anderson DJ. The bHLH transcription factors OLIG2 and OLIG1 couple neuronal and glial subtype specification. *Cell*. 2002;109(1):61-73. doi:10.1016/s0092-8674(02)00677-3

33. Fong BC, Chakroun I, Iqbal MA, et al. The Rb/E2F axis is a key regulator of the molecular signatures instructing the quiescent and activated adult neural stem cell state. *Cell Rep*. 2022;41(5):111578. doi:10.1016/j.celrep.2022.111578

34. Jantaratnotai N, Ling A, Cheng J, Schwab C, McGeer PL, McLarnon JG. Upregulation and expression patterns of the angiogenic transcription factor ets-1 in Alzheimer's disease brain. *J Alzheimers Dis*. 2013;37(2):367-377. doi:10.3233/JAD-122191

35. Zu S, Li YE, Wang K, et al. Single-cell analysis of chromatin accessibility in the adult mouse brain. *Nature*. 2023;624(7991):378-389. doi:10.1038/s41586-023-06824-9

36. Du AY, Chobirko JD, Zhuo X, Feschotte C, Wang T. Regulatory transposable elements in the encyclopedia of DNA elements. *Nat Commun*. 2024;15(1):7594. doi:10.1038/s41467-024-51921-6

37. Chuong EB, Elde NC, Feschotte C. Regulatory activities of transposable elements: from conflicts to benefits. *Nat Rev Genet*. 2017;18(2). doi:10.1038/nrg.2016.139

38. Jönsson ME, Garza R, Sharma Y, et al. Activation of endogenous retroviruses during brain development causes an inflammatory response. *EMBO J*. 2021;40(9):e106423. doi:10.15252/embj.2020106423

39. Sankowski R, Strohl JJ, Huerta TS, et al. Endogenous retroviruses are associated with hippocampus-based memory impairment. *Proc Natl Acad Sci U S A*. 2019;116(51):25982-25990. doi:10.1073/pnas.1822164116

40. Du H, Wang Z, Guo R, et al. Transcription factors Bcl11a and Bcl11b are required for the production and differentiation of cortical projection neurons. *Cereb Cortex*. 2022;32(17):3611-3632. doi:10.1093/cercor/bhab437

41. Kim EJ, Leung CT, Reed RR, Johnson JE. In vivo analysis of Ascl1 defined progenitors reveals distinct developmental dynamics during adult neurogenesis and gliogenesis. *J Neurosci*. 2007;27(47):12764-12774. doi:10.1523/JNEUROSCI.3178-07.2007

42. Beckmann AM, Wilce PA. Egr transcription factors in the nervous system. *Neurochem Int*. 1997;31(4):477-510. doi:10.1016/S0197-0186(96)00136-2

43. Moore DL, Apara A, Goldberg JL. Krüppel-like transcription factors in the nervous system: novel players in neurite outgrowth and axon regeneration. *Mol Cell Neurosci*. 2011;47(4):233-243. doi:10.1016/j.mcn.2011.05.005

44. Gallo FT, Katche C, Morici JF, Medina JH, Weisstaub N V. Immediate Early Genes, Memory and Psychiatric Disorders: Focus on c-Fos, Egr1 and Arc. *Front Behav Neurosci*. 2018;12. doi:10.3389/fnbeh.2018.00079

45. O'Donovan KJ, Tourtellotte WG, Millbrandt J, Baraban JM. The EGR family of transcription-regulatory factors: progress at the interface of molecular and systems neuroscience. *Trends Neurosci*. 1999;22(4):167-173. doi:10.1016/S0166-2236(98)01343-5

46. Loureiro-Campos E, Mateus-Pinheiro A, Patrício P, et al. Constitutive deficiency of the neurogenic hippocampal modulator AP2γ promotes anxiety-like behavior and cumulative memory deficits in mice from juvenile to adult periods. *Elife*. 2021;10. doi:10.7554/eLife.70685

47. Impey S, Obrietan K, Storm DR. Making new connections: role of ERK/MAP kinase signaling in neuronal plasticity. *Neuron*. 1999;23(1):11-14. doi:10.1016/s0896-6273(00)80747-3

48. Pittenger C, Huang YY, Paletzki RF, et al. Reversible inhibition of CREB/ATF transcription factors in region CA1 of the dorsal hippocampus disrupts hippocampus-dependent spatial memory. *Neuron*. 2002;34(3):447-462. doi:10.1016/s0896-6273(02)00684-0

49. Dean C, Liu H, Dunning FM, Chang PY, Jackson MB, Chapman ER. Synaptotagmin-IV modulates synaptic function and long-term potentiation by regulating BDNF release. *Nat Neurosci*. 2009;12(6):767-776. doi:10.1038/nn.2315

50. Müller T, Braud S, Jüttner R, et al. Neuregulin 3 promotes excitatory synapse formation on hippocampal interneurons. *EMBO J*. 2018;37(17). doi:10.15252/embj.201798858

51. Podbevšek P, Fasolo F, Bon C, et al. Structural determinants of the SINE B2 element embedded in the long non-coding RNA activator of translation AS Uchl1. *Sci Rep*. 2018;8(1):3189. doi:10.1038/s41598-017-14908-6

52. Linker SB, Randolph-Moore L, Kottilil K, et al. Identification of bona fide B2 SINE retrotransposon transcription through single-nucleus RNA-seq of the mouse hippocampus. *Genome Res*. 2020;30(11):1643-1654. doi:10.1101/gr.262196.120

53. Nacher J, Varea E, Blasco-Ibañez JM, et al. Expression of the transcription factor Pax 6 in the adult rat dentate gyrus. *J Neurosci Res*. 2005;81(6):753-761. doi:10.1002/jnr.20596

54. Andersen J, Urbán N, Achimastou A, et al. A transcriptional mechanism integrating inputs from extracellular signals to activate hippocampal stem cells. *Neuron*. 2014;83(5):1085-1097. doi:10.1016/j.neuron.2014.08.004

55. Lin HC, Ching YH, Huang CC, et al. Promyelocytic leukemia zinc finger is involved in the formation of deep layer cortical neurons. *J Biomed Sci*. 2019;26(1):30. doi:10.1186/s12929-019-0519-8

56. Lu C, Garipler G, Dai C, et al. Essential transcription factors for induced neuron differentiation. *Nat Commun*. 2023;14(1):8362. doi:10.1038/s41467-023-43602-7

57. Fleck JS, Jansen SMJ, Wollny D, et al. Inferring and perturbing cell fate regulomes in human brain organoids. *Nature*. 2023;621(7978):365-372. doi:10.1038/s41586-022-05279-8

58. Nishihara H, Smit AFA, Okada N. Functional noncoding sequences derived from SINEs in the mammalian genome. *Genome Res*. 2006;16(7):864-874. doi:10.1101/gr.5255506

59. McCarthy EM, McDonald JF. Long terminal repeat retrotransposons of Mus musculus. *Genome Biol*. 2004;5(3):R14. doi:10.1186/gb-2004-5-3-r14

60. Jurka J, Zietkiewicz E, Labuda D. Ubiquitous mammalian-wide interspersed repeats (MIRs) are molecular fossils from the mesozoic era. *Nucleic Acids Res*. 1995;23(1):170-175. doi:10.1093/nar/23.1.170

61. Fueyo R, Judd J, Feschotte C, Wysocka J. Roles of transposable elements in the regulation of mammalian transcription. *Nat Rev Mol Cell Biol*. 2022;23(7):481-497. doi:10.1038/s41580-022-00457-y

62. Notwell JH, Chung T, Heavner W, Bejerano G. A family of transposable elements co-opted into developmental enhancers in the mouse neocortex. *Nat Commun*. 2015;6:6644. doi:10.1038/ncomms7644

63. Wenger AM, Clarke SL, Notwell JH, et al. The enhancer landscape during early neocortical development reveals patterns of dense regulation and co-option. *PLoS Genet*. 2013;9(8):e1003728. doi:10.1371/journal.pgen.1003728

64. Singh M, Leddy SM, Iñiguez LP, Bendall ML, Nixon DF, Feschotte C. Transposable elements may enhance antiviral resistance in HIV-1 elite controllers. *Genome Biol*. 2025;26(1):28. doi:10.1186/s13059-025-03484-y

65. Sekine K, Onoguchi M, Hamada M. Transposons contribute to the acquisition of cell type-specific cis-elements in the brain. *Commun Biol*. 2023;6(1):631. doi:10.1038/s42003-023-04989-7

66. Hirakawa M, Nishihara H, Kanehisa M, Okada N. Characterization and evolutionary landscape of AmnSINE1 in Amniota genomes. *Gene*. 2009;441(1-2):100-110. doi:10.1016/j.gene.2008.12.009

67. Lein ES, Hawrylycz MJ, Ao N, et al. Genome-wide atlas of gene expression in the adult mouse brain. *Nature*. 2007;445(7124):168-176. doi:10.1038/nature05453

68. Altman J, Das GD. Postnatal neurogenesis in the guinea-pig. *Nature*. 1967;214(5093):1098-1101. doi:10.1038/2141098a0

69. Altman J, Das GD. Autoradiographic and histological evidence of postnatal hippocampal neurogenesis in rats. *J Comp Neurol*. 1965;124(3):319-335. doi:10.1002/cne.901240303

70. Eriksson PS, Perfilieva E, Björk-Eriksson T, et al. Neurogenesis in the adult human hippocampus. *Nat Med*. 1998;4(11):1313-1317. doi:10.1038/3305

71. Dumitru I, Paterlini M, Zamboni M, et al. Identification of proliferating neural progenitors in the adult human hippocampus. *Science*. 2025;389(6755):58-63. doi:10.1126/science.adu9575

72. Mengozzi M, Cervellini I, Villa P, et al. Erythropoietin-induced changes in brain gene expression reveal induction of synaptic plasticity genes in experimental stroke. *Proc Natl Acad Sci U S A*. 2012;109(24):9617-9622. doi:10.1073/pnas.1200554109

73. Mennen S, Franta M, Begemann M, et al. Tolerability and first hints for potential efficacy of motor-cognitive training under inspiratory hypoxia in health and neuropsychiatric disorders: A translational viewpoint. *Neuroprotection*. Published online June 4, 2024. doi:10.1002/nep3.47

74. Miskowiak K, O'Sullivan U, Harmer CJ. Erythropoietin Enhances Hippocampal Response during Memory Retrieval in Humans. *Journal of Neuroscience*. 2007;27(11):2788-2792. doi:10.1523/JNEUROSCI.5013-06.2007

75. Sakanaka M, Wen TC, Matsuda S, et al. *In vivo* evidence that erythropoietin protects neurons from ischemic damage. *Proceedings of the National Academy of Sciences*. 1998;95(8):4635-4640. doi:10.1073/pnas.95.8.4635

76. Coufal NG, Garcia-Perez JL, Peng GE, et al. L1 retrotransposition in human neural progenitor cells. *Nature*. 2009;460(7259):1127-1131. doi:10.1038/nature08248

77. Gonçalves JT, Schafer ST, Gage FH. Adult Neurogenesis in the Hippocampus: From Stem Cells to Behavior. *Cell*. 2016;167(4):897-914. doi:10.1016/j.cell.2016.10.021

78. Lin WT, Chao CM, Lin HL, Hung MC, Lai CC. Emergence of antibiotic-resistant bacteria in patients with Fournier gangrene. *Surg Infect (Larchmt)*. 2015;16(2):165-168. doi:10.1089/sur.2013.118

79. Feschotte C. Transposable elements and the evolution of regulatory networks. *Nat Rev Genet*. 2008;9(5). doi:10.1038/nrg2337

80. Wang L, Zhang Z, Wang Y, Zhang R, Chopp M. Treatment of Stroke With Erythropoietin Enhances Neurogenesis and Angiogenesis and Improves Neurological Function in Rats. *Stroke*. 2004;35(7):1732-1737. doi:10.1161/01.STR.0000132196.49028.a4

## Acknowledgements

This work has been supported by the European Research Council (ERC) Advanced Grant to HE under the European Union's Horizon Europe research and innovation programme (acronym *BREPOCI;* grant agreement No 101054369), as well as by the Max Planck Society, the Max Planck Förderstiftung, the Deutsche Forschungsgemeinschaft (DFG, German Research Foundation), via DFG-Center for Nanoscale Microscopy & Molecular Physiology of the Brain (CNMPB). Research in the labs of HE and KAN is funded by DFG TRR-274 /1 2020 – 408885537. UC received support from the IMPRS-Genome Science PhD program. Research in the labs of DG, RK and KAN is supported by the Adelson Medical Research Foundation.

## Author Contributions

Concept, design, supervision: MS, HE

Funding acquisition: HE,RK,DG,KAN

Drafting manuscript and display items: UC,MS,MF, UJB, HE

Data acquisition/generation: RK,DG,KAN

Data analyses & interpretation: UC,RK,MS,HE

**All authors read and approved the final version of the manuscript.**

## Competing Interests:

The authors declare no competing financial or other interests in connection with this article.

## FIGURE LEGENDS

**Figure 1.**

**Integrated single-nucleus transcriptomic and chromatin-accessibility atlas of mouse hippocampus after rhEPO treatment**

(A) C57BL/6 mice received recombinant human erythropoietin (rhEPO) or placebo every other day from postnatal day (P) 28 to P49. Hippocampal regions were dissected, and nuclei were isolated for single-nucleus RNA-seq (snRNA-seq) and single-nucleus ATAC-seq (snATAC-seq). The resulting datasets were jointly analysed to integrate gene expression and chromatin accessibility. Data processing included Cell Ranger peak calling, Signac-based quality control and preprocessing, Harmony batch correction, co-embedding snRNA-seq and snATAC-seq, cell-type annotation, differential accessibility testing, motif enrichment, gene regulatory network reconstruction, and identification of gene- and transposable element (TE)-associated candidate cis-regulatory elements (cCREs).

(B) UMAP projection of the snATAC-seq dataset coloured by 35 unbiased Seurat clusters.

(C) Joint embedding of snATAC-seq and snRNA-seq using gene activity and expression. Left: UMAP projection of integrated nuclei, with snATAC-seq (red) and snRNA-seq (blue) showing strong overlap following CCA-based integration of ATAC-derived gene activity scores and RNA expression. Right: same embedding coloured by major cell types assigned via label transfer and canonical markers, including pyramidal neurons (Pyr), dentate gyrus neurons (DG), interneurons (In), oligodendrocytes (Oli), astrocytes (Ast), microglia (Mic), endothelial cells (End), intermediate progenitors (Int), pericytes (Per), ependymal cells (Epd), and neuroimmune cells (NI).

(D) Violin plots of prediction scores for cell-type assignments obtained by label transfer from snRNA-seq to snATAC-seq. Each violin represents a major hippocampal cell type, while the final column in the lower panel shows the overall distribution across all types. The dashed line marks the median overall prediction score, illustrating high cross-modality annotation accuracy.

(E) UMAP projection of the snATAC-seq dataset, coloured by cell-type identities transferred from the matched snRNA-seq reference shown in panel C.

(F) Heatmap of differentially accessible chromatin regions (DARs, rows) across hippocampal cell types (columns). Scaled accessibility values (red/yellow = high, blue = low) highlight distinct cis-regulatory signatures for each lineage. For visualization, the top 20 peaks per cell type are shown.

(G) Genome browser tracks showing chromatin accessibility at the Slc17a7, Mog, Plp1, and Slc1a2 loci across major hippocampal cell types. Highlighted regions mark cell-type-restricted accessible regions, illustrating lineage-specific regulatory landscapes.

**Figure 2.**

**Cell-type TF motif usage and TE architecture of accessible chromatin**

(A) Heatmap of significantly enriched transcription factor (TF) motifs (fold-enrichment > 1.5; FDR < $1 \times 10^{-1}$) in cell-type–specific DARs. Rows correspond to seven major hippocampal cell types and columns to representative motifs (colour scale = $-\log_{10}$ adjusted p-value). The remaining four cell types are not shown due to limited motif detection resulting from their comparatively lower cell numbers.

(B) Genomic distribution of (i) all annotated TEs in the mouse genome, (ii) all snATAC-seq peaks identified in this study (225,618 summits), and (iii) the subset of peaks overlapping TE sequences (39,009 summits). Bars indicate the percentage of features located in distal intergenic, intronic, exonic, promoter (<1 kb, 1–2 kb, or 2–3 kb), downstream, or UTR regions. Right: overlap of snATAC-seq peaks with CATlas, showing 201,210 overlapping peaks (black) and 24,408 non-overlapping peaks (grey).

(C) Venn diagram summarising the intersection between peaks that map to gene bodies (112,456), TEs (17,728), or both (21,281).

(D) Bar chart of the TE families at peak summits, coloured by TE class (LTR, SINE, LINE, simple repeat, DNA, other, and unknown).

(E) The scatter plot shows $\log_2$(observed/expected) overlaps for each TE family versus $-\log_{10}$ p-value. The right plot compares observed to expected counts for the top significantly enriched families highlighted in the left plot.

**Figure 3.**

**rhEPO remodels chromatin accessibility and engages neurogenic regulators.**

(A) Volcano plot of DARs between rhEPO- and placebo-treated hippocampi, identifying 976 DARs (816 gained, 160 lost). Neurogenic regulators (Ascl1, Dnmt3a, Nrg3, Egr2) are highlighted.

(B) A total of 1,058 DARs (FDR < 0.01) were identified and grouped into three categories: promoter-proximal (within ±1 kb of a TSS), TE-associated (DARs overlapping TEs within ±1 kb of a TSS), and distal cis-regulatory elements (>500 bp from a TSS). The bar plot and accompanying UpSet diagram summarize the counts per category, with schematic illustrations on the left indicating classification criteria.

(C) Gene ontology enrichment of DAR-associated genes, with significant terms related to synaptic plasticity, neurogenesis, and neurite morphology.

(D) Motif enrichment analysis of DARs, revealing over-representation of TFs including KLFs, EGR1–3, ASCL1, NRF1, SP-family factors, and TBR1.

(E) Scatter plot of differentially expressed genes from snATAC-seq inferred from gene activity and differentially expressed genes (DEGs, from snRNA-seq). $\text{Log}_2$ fold changes (rhEPO vs placebo) show strong concordance ($R = 0.68$, $p = 1.5 \times 10^{-3}$), with representative neurogenic genes (Nrg3, Syt4, Egr2, Nrp1) highlighted.

(F) Bar plot showing the number of unique genes with TSS located within ±1 kb of TE-derived DARs. Rodent-specific B1 SINE subfamilies (B1_Mus1, B1_Mur1, B1_Mur4, ID_B1) are the most frequent contributors, linking TE-derived accessibility to gene regulation.

**Figure 4.**

**rhEPO selectively remodels chromatin accessibility, transposon usage, and TF programs across hippocampal cell types.**

(A) Global view of DARs (FDR < 0.01) between rhEPO- and placebo-treated nuclei. Horizontal bars indicate the number of DARs identified in each lineage (colour legend, left); the UpSet matrix to the right shows how many DARs are unique or shared across lineages.

(B) Stacked bars show, for each hippocampal lineage, the total number of DARs (light blue), the subset overlapping TEs (green), and the subset located within ±1 kb of gene TSSs (dark blue). Bars extending upward represent DARs with increased accessibility in rhEPO-treated samples, while downward bars indicate reduced accessibility compared with placebo.

(C) Heatmap of rhEPO-induced promoter accessibility changes at selected neurogenic genes across hippocampal lineages. Colors indicate $\log_2$ fold change (EPO vs placebo), with red showing increased and blue decreased accessibility. Asterisks denote significant changes (FDR < 0.01).

(D) Stacked bars show the proportion of regulons inferred by Pando that are shared, rhEPO-specific, or placebo-specific within each lineage. The dot plot on the right summarizes the absolute number of differential regulons, with orange indicating rhEPO-specific and green placebo-specific regulons.

(E) TE-enrichment analysis for rhEPO-responsive DARs. The left scatter plot depicts $\log_2$(observed/expected) overlaps versus $-\log_{10}P$ for every annotated TE family (points coloured by TE class; dashed boxes mark the top significantly enriched families). The right scatter plot compares observed to expected counts for the top significant families.

(F) Genome browser snapshots of rhEPO-induced chromatin accessibility at TE-derived regulatory elements. In pyramidal neurons, increased accessibility was observed at an L2c element near Phf24 and at MIR and MER103C elements near Cpne5. In astrocytes, a B1_Mur4 element near Haus6 showed enhanced accessibility. Tracks display snATAC-seq signal for rhEPO (red) and placebo (blue), with genes (grey) and TEs (red) shown below.

**Figure 5.**

**Pyramidal cell type-specific chromatin remodelling provoked by rhEPO**

(A) Left: Joint UMAP embedding of pyramidal-lineage nuclei profiled by snATAC-seq (red) and snRNA-seq (blue). Right: UMAP of the same nuclei colored by clusters annotated through label transfer and marker gene activity, resolving newly formed neurons, mature pyramidal neurons, and other subtypes (e.g., mossy, NP SUB, Cajal-like cells).

(B) Volcano plot of DARs between newly formed and mature pyramidal neurons (FDR < 0.01). A total of 7,420 DARs were identified, including 4,315 with increased accessibility and 3,105 with reduced accessibility in newly formed neurons.

(C) Gene ontology enrichment analysis of promoter DARs upregulated in newly formed neurons. Significant terms (-log10p > 10) highlight processes linked to synapse organization, neurogenesis, learning, memory, and membrane potential and neuronal compartments (dendrite, synapse, distal axon, and synaptic membrane).

(D) Numbers of DARs in newly formed and mature neurons (rhEPO vs placebo), shown for all DARs (left), promoter-proximal gene-TSS DARs (middle), and TE-derived DARs (right). Newly formed neurons exhibit higher counts across all categories.

(E) Proportional distribution of DARs from panel D. In both newly formed and mature neurons, the majority of DARs are upregulated (pink), while a smaller fraction is downregulated (blue), indicating that rhEPO predominantly increases chromatin accessibility.

(F) Genomic distribution of EPO-responsive DARs in newly formed neurons relative to the nearest TSS. DARs are classified as promoter-proximal (≤1 kb, blue), distal promoter (1–10 kb, green), or intergenic/intronic (>10 kb, grey).

(G) Distance of significant DAR summits to the nearest TSS for selected neurogenic and synaptic genes in newly formed neurons. Each dot represents the nearest DAR to a gene TSS, colored by $\log_2$ fold change (red = increased, blue = decreased accessibility).

**Figure 6.**

**TE-derived DARs and their association with neurogenic TFs and gene regulation**

(A) Numbers of TE-derived DARs (rhEPO vs placebo) in newly formed and mature neurons, separated into proximal cis-regulatory elements (cCREs within 10 kb of a gene TSS, blue) and distal cCREs (>10 kb from a gene TSS, grey). Newly formed neurons harbor more TE-derived DARs than mature neurons.

(B) Bar chart ranking neurogenic TFs by the number of TE families significantly enriched within their ChIP-seq binding sites. Each bar represents the total count of enriched TE families associated with the indicated TF.

(C) Matrix of significantly enriched TE families across TF ChIP-seq datasets. Black squares denote significant enrichment ($p < 0.001$), white squares denote no significant enrichment ($p > 0.001$). TE families such as L2b, L2, MIRb, and MIR3 are strongly associated with multiple neurogenic TFs.

(D) Neighboring genes within ±10 kb of selected TE-derived DARs (rhEPO vs placebo) that were accessible in >10% of pyramidal nuclei. Each circle represents the closest DAR relative to the TSS, with position on the y-axis showing distance (kb) from the TSS, and color indicating $\log_2$ fold change (red = increased, blue = decreased accessibility under rhEPO).

(E) Concordance between TE-derived DARs bound by neurogenic TFs and their nearest genes. Left, genomic coordinates of DARs identified by snATAC-seq, with color scale indicating $\log_2$ fold change (rhEPO vs placebo). Right, heatmaps of matched gene expression from snRNA-seq across hippocampal cell types. Asterisks denote significant transcriptional changes (FDR < 0.01), showing coordinated chromatin accessibility and expression responses to rhEPO.

(F) Genome browser snapshots showing TE-derived DARs near neurogenic genes. Representative loci include Nptxr, Ckb, and Nfx1. Tracks display chromatin accessibility across major hippocampal lineages, with dashed boxes marking TE-overlapping elements that show lineage-restricted accessibility. Genes are shown in black, with TEs highlighted in red.

**Figure 7.**

**Neurogenic transcription factors FOXG1, NEUROD1, and NEUROD2 exhibit selective binding to transposable-element–derived sequences**

(A) FOXG1 ChIP-seq shows aggregate ChIP-seq signal profiles (top) and corresponding heatmaps (bottom) centered on representative repeat element families (MER58A, L3, MIR, MER130). “Positive” (Pos, blue) represents transposable elements overlapping FOXG1 ChIP-seq peaks, whereas “Negative” (Neg, green) indicates transposable elements without peaks. Each heatmap displays signal density within ±2 kb of the element center, revealing distinct FOXG1 enrichment over specific TE subfamilies.

(B) NEUROD1 ChIP-seq shows aggregate signal profiles and heatmaps demonstrating pronounced NEUROD1 binding across the same TE families (MER58A, L3, MIR, MER130).

(C) NEUROD2 ChIP-seq shows meta-profiles and heatmaps depicting NEUROD2 binding over the same TE families. Altogether, these analyses demonstrate that ancient transposable-element subfamilies function as conserved cis-regulatory modules co-opted into the neurogenic transcriptional program.

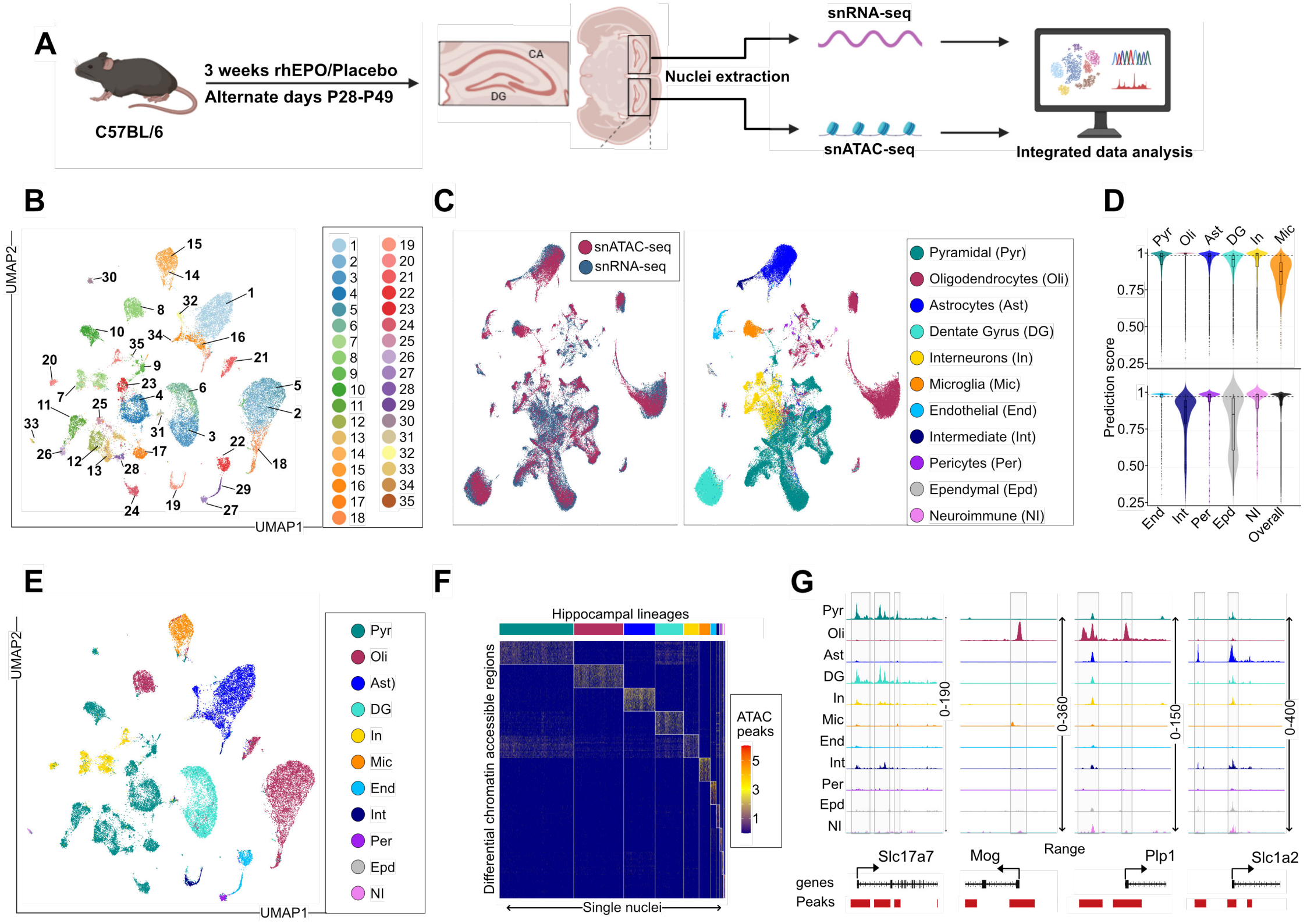
A
C57BL/6
3 weeks rhEPO/Placebo
Alternate days P28-P49
CA
DG
Nuclei extraction
snRNA-seq
snATAC-seq
Integrated data analysis
B
UMAP2
UMAP1
C
snATAC-seq
snRNA-seq
Pyramidal (Pyr)
Oligodendrocytes (Oli)
Astrocytes (Ast)
Dentate Gyrus (DG)
Interneurons (In)
Microglia (Mic)
Endothelial (End)
Intermediate (Int)
Pericytes (Per)
Ependymal (Epd)
Neuroimmune (NI)
D
Pyr
Oli
Ast
DG
In
Mic
Prediction score
End
Int
Per
Epd
NI
Overall
E
UMAP2
UMAP1
Pyr
Oli
Ast)
DG
In
Mic
End
Int
Per
Epd
NI
F
Hippocampal lineages
Differential chromatin accessible regions
Single nuclei
ATAC peaks
G
Pyr
Oli
Ast
DG
In
Mic
End
Int
Per
Epd
NI
0-190
0-360
0-150
0-400
Range
Slc17a7
Mog
Plp1
Slc1a2
genes
Peaks

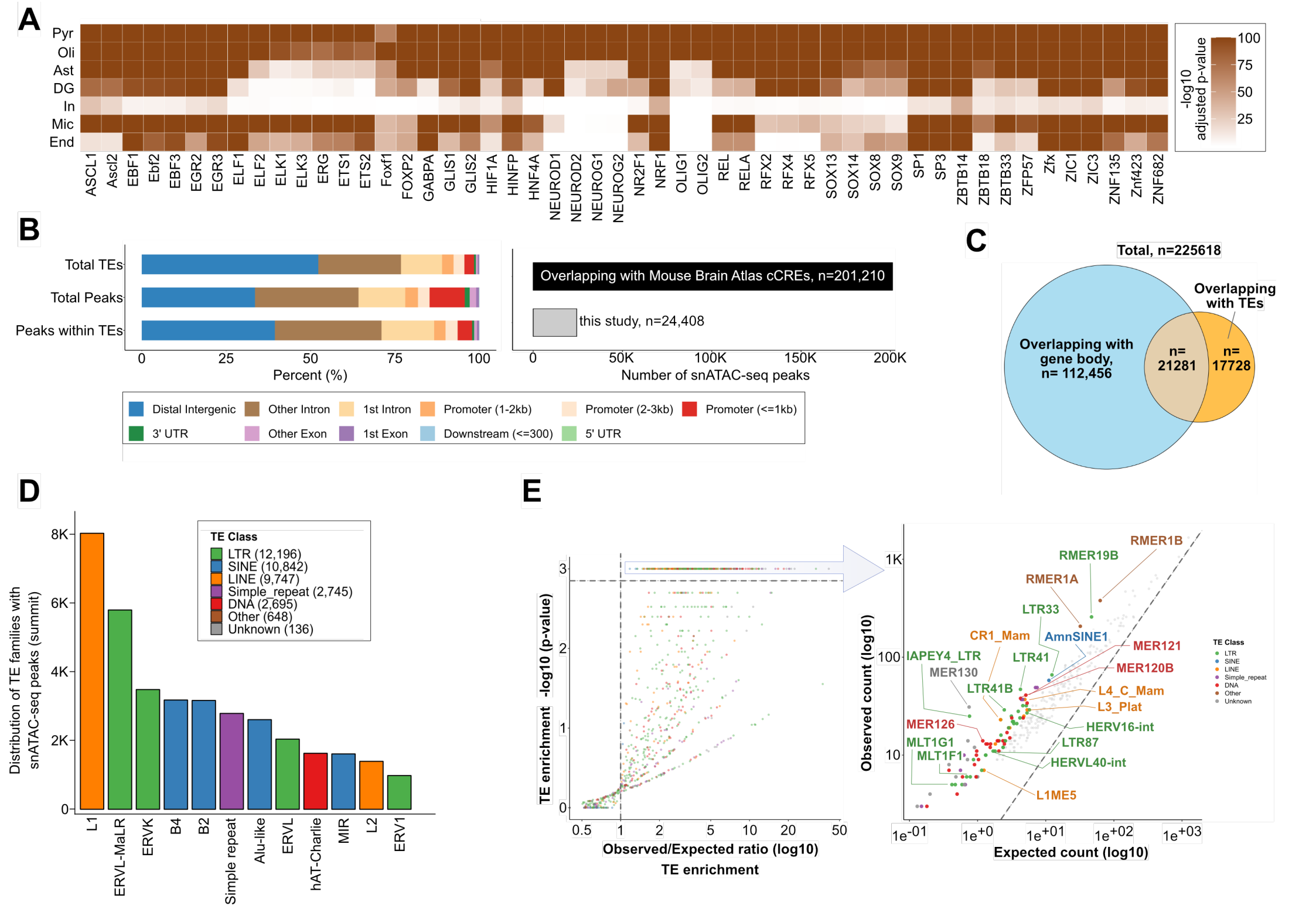
A
Pyr
Oli
Ast
DG
In
Mic
End
ASCL1 Ascl2 EBF1 Ebf2 EBF3 EGR2 EGR3 ELF1 ELF2 ELK1 ELK3 ERG ETS1 ETS2 Foxf1 FOXP2 GABPA GLIS1 GLIS2 HIF1A HINFP HNF4A NEUROD1 NEUROD2 NEUROG1 NEUROG2 NR2F1 NRF1 OLIG1 OLIG2 REL RELA RFX2 RFX4 RFX5 SOX13 SOX14 SOX8 SOX9 SP1 SP3 ZBTB14 ZBTB18 ZBTB33 ZFP57 Zfx ZIC1 ZIC3 ZNF135 Znf423 ZNF682
-log10 adjusted p-value
100
75
50
25
B
Total TEs
Total Peaks
Peaks within TEs
0
25
50
75
100
Percent (%)
Overlapping with Mouse Brain Atlas cCREs, n=201,210
this study, n=24,408
0
50K
100K
150K
200K
Number of snATAC-seq peaks
Distal Intergenic
Other Intron
1st Intron
Promoter (1-2kb)
Promoter (2-3kb)
Promoter (<=1kb)
3' UTR
Other Exon
1st Exon
Downstream (<=300)
5' UTR
C
Total, n=225618
Overlapping with TEs
Overlapping with gene body, n= 112,456
n= 21281
n= 17728
D
Distribution of TE families with snATAC-seq peaks (summit)
8K
6K
4K
2K
0
TE Class
LTR (12,196)
SINE (10,842)
LINE (9,747)
Simple_repeat (2,745)
DNA (2,695)
Other (648)
Unknown (136)
L1
ERVL-MaLR
ERVK
B4
B2
Simple repeat
Alu-like
ERVL
hAT-Charlie
MIR
L2
ERV1
E
TE enrichment -log10 (p-value)
3
2
1
0
0.5
1
2
5
10
20
50
Observed/Expected ratio (log10)
TE enrichment
Observed count (log10)
1K
100
10
1e-01
1e+0
1e+01
1e+02
1e+03
Expected count (log10)
RMER1B
RMER19B
RMER1A
LTR33
CR1_Mam
AmnSINE1
MER121
IAPEY4_LTR
LTR41
MER120B
MER130
LTR41B
L4_C_Mam
L3_Plat
MER126
HERV16-int
MLT1G1
LTR87
MLT1F1
HERVL40-int
L1ME5
TE Class
LTR
SINE
LINE
Simple_repeat
DNA
Other
Unknown

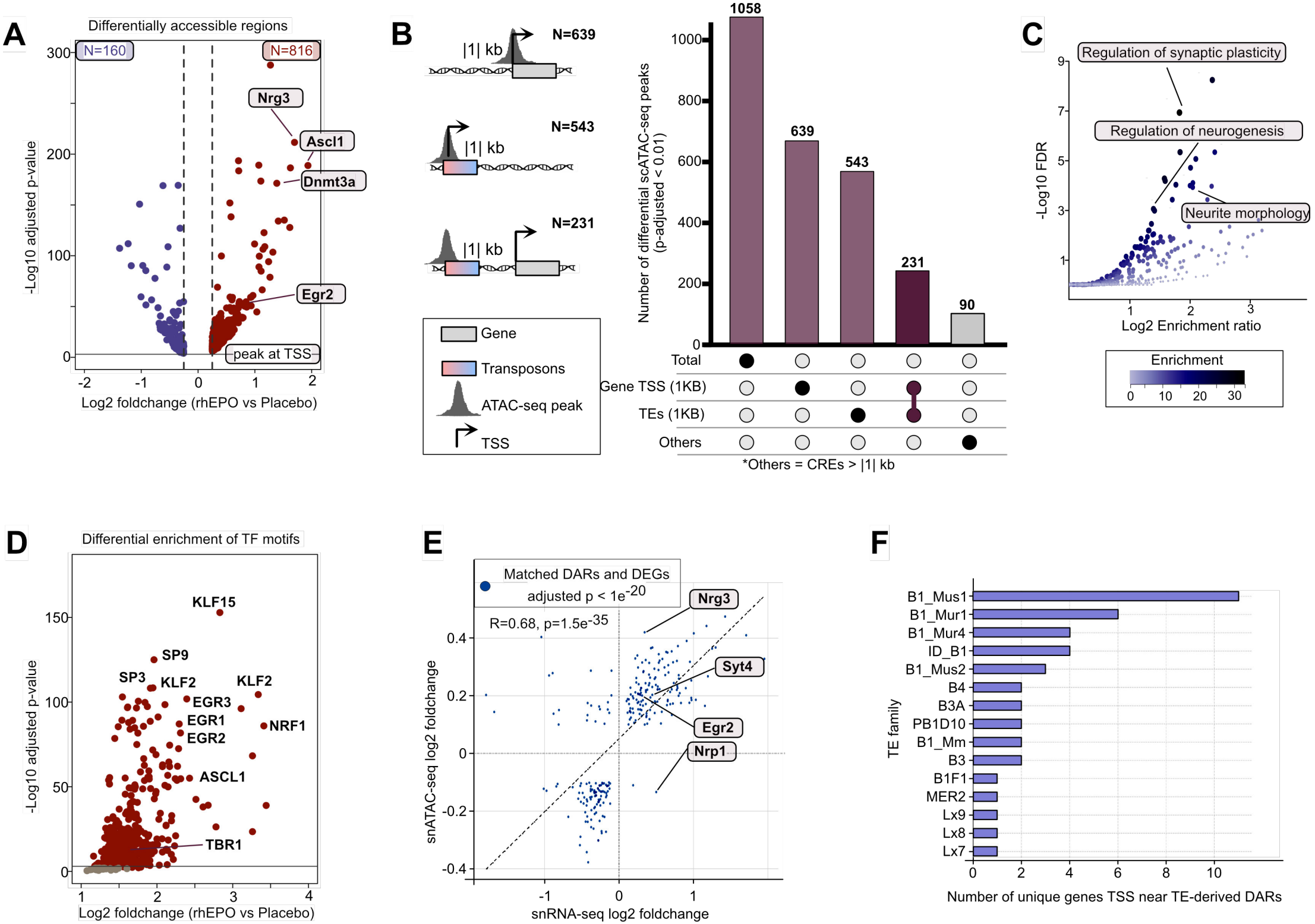
A
Differentially accessible regions
N=160
N=816
Nrg3
Ascl1
Dnmt3a
Egr2
peak at TSS
-Log10 adjusted p-value
Log2 foldchange (rhEPO vs Placebo)
B
N=639
N=543
N=231
|1| kb
Gene
Transposons
ATAC-seq peak
TSS
1058
639
543
231
90
Number of differential scATAC-seq peaks (p-adjusted < 0.01)
Total
Gene TSS (1KB)
TEs (1KB)
Others
*Others = CREs > |1| kb
C
Regulation of synaptic plasticity
Regulation of neurogenesis
Neurite morphology
-Log10 FDR
Log2 Enrichment ratio
Enrichment
D
Differential enrichment of TF motifs
KLF15
SP9
SP3
KLF2
KLF2
EGR3
EGR1
EGR2
NRF1
ASCL1
TBR1
-Log10 adjusted p-value
Log2 foldchange (rhEPO vs Placebo)
E
Matched DARs and DEGs
adjusted p < 1e-20
R=0.68, p=1.5e-35
Nrg3
Syt4
Egr2
Nrp1
snATAC-seq log2 foldchange
snRNA-seq log2 foldchange
F
B1_Mus1
B1_Mur1
B1_Mur4
ID_B1
B1_Mus2
B4
B3A
PB1D10
B1_Mm
B3
B1F1
MER2
Lx9
Lx8
Lx7
TE family
Number of unique genes TSS near TE-derived DARs

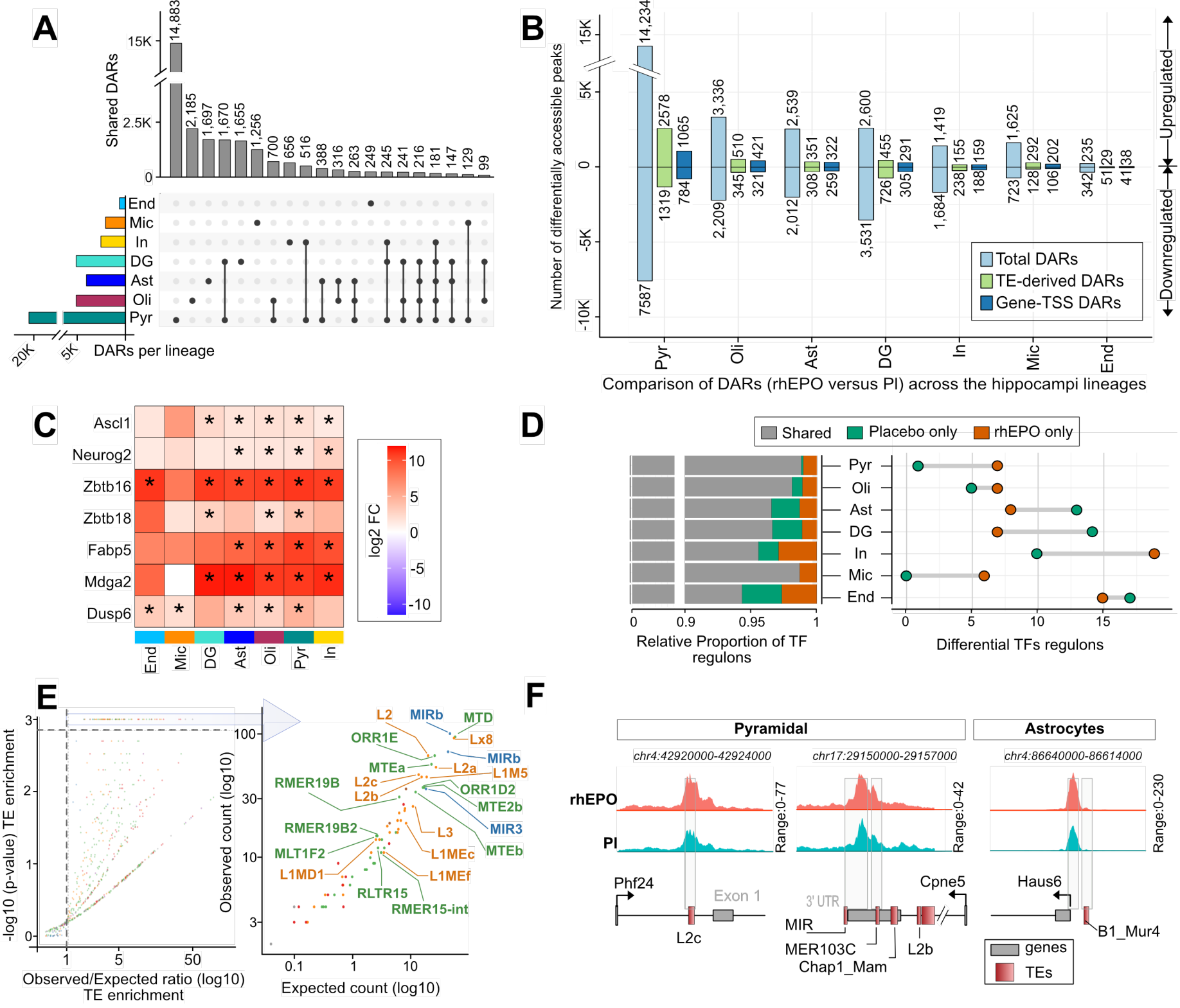
A
Shared DARs
15K
2.5K
0
14,883
2,185
1,697
1,670
1,655
1,256
700
656
516
388
316
263
249
245
241
216
181
147
129
99
End
Mic
In
DG
Ast
Oli
Pyr
20K
5K
DARs per lineage
B
Number of differentially accessible peaks
15K
5K
0
-5K
-10K
14,234
7587
2578
1319
1065
784
3,336
2,209
510
345
421
321
2,539
2,012
351
308
322
259
2,600
3,531
455
726
291
305
1,419
1,684
155
238
159
188
1,625
723
292
128
202
106
235
342
29
51
38
41
Total DARs
TE-derived DARs
Gene-TSS DARs
Upregulated
Downregulated
Pyr
Oli
Ast
DG
In
Mic
End
Comparison of DARs (rhEPO versus PI) across the hippocampi lineages
C
Ascl1
Neurog2
Zbtb16
Zbtb18
Fabp5
Mdga2
Dusp6
log2 FC
10
5
0
-5
-10
End
Mic
DG
Ast
Oli
Pyr
In
D
Shared
Placebo only
rhEPO only
Pyr
Oli
Ast
DG
In
Mic
End
0
0.9
0.95
1
Relative Proportion of TF regulons
0
5
10
15
Differential TFs regulons
E
-log10 (p-value) TE enrichment
3
2
1
0
1
5
50
Observed/Expected ratio (log10) TE enrichment
Observed count (log10)
100
30
10
3
0.1
1
10
Expected count (log10)
L2
MIRb
MTD
Lx8
ORR1E
MIRb
MTEa
L2a
L1M5
RMER19B
L2c
L2b
ORR1D2
MTE2b
MIR3
RMER19B2
L3
MLT1F2
L1MEc
MTEb
L1MD1
L1MEf
RLTR15
RMER15-int
F
Pyramidal
Astrocytes
chr4:42920000-42924000
chr17:29150000-29157000
chr4:86640000-86614000
rhEPO
PI
Range:0-77
Range:0-42
Range:0-230
Phf24
Exon 1
L2c
3' UTR
Cpne5
MIR
MER103C
Chap1_Mam
L2b
Haus6
B1_Mur4
genes
TEs

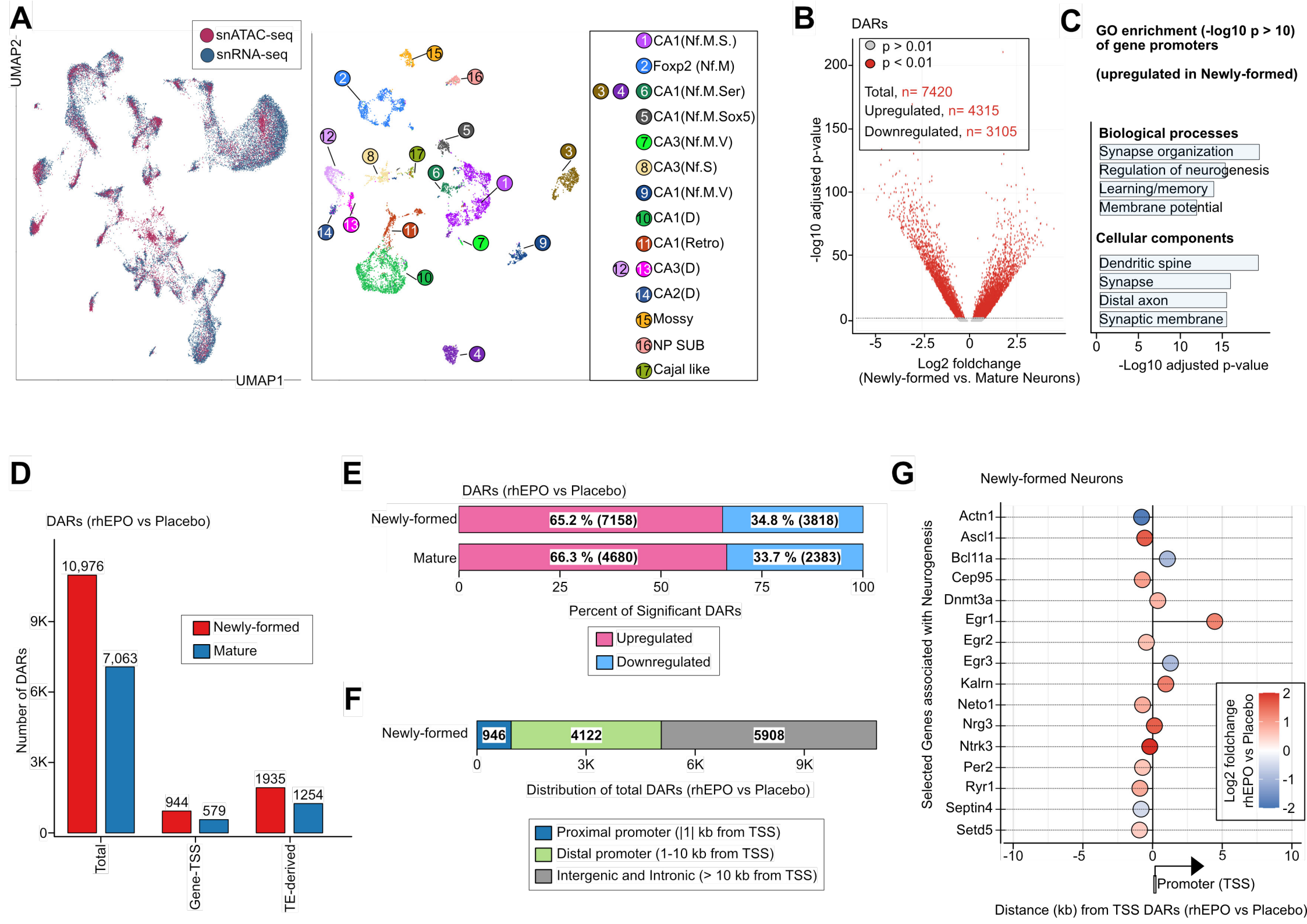
A
snATAC-seq
snRNA-seq
UMAP2
UMAP1
1 CA1(Nf.M.S.)
2 Foxp2 (Nf.M)
3 4 6 CA1(Nf.M.Ser)
5 CA1(Nf.M.Sox5)
7 CA3(Nf.M.V)
8 CA3(Nf.S)
9 CA1(Nf.M.V)
10 CA1(D)
11 CA1(Retro)
12 13 CA3(D)
14 CA2(D)
15 Mossy
16 NP SUB
17 Cajal like
B
DARs
p > 0.01
p < 0.01
Total, n= 7420
Upregulated, n= 4315
Downregulated, n= 3105
-log10 adjusted p-value
Log2 foldchange
(Newly-formed vs. Mature Neurons)
C
GO enrichment (-log10 p > 10)
of gene promoters
(upregulated in Newly-formed)
Biological processes
Synapse organization
Regulation of neurogenesis
Learning/memory
Membrane potential
Cellular components
Dendritic spine
Synapse
Distal axon
Synaptic membrane
-Log10 adjusted p-value
D
DARs (rhEPO vs Placebo)
Number of DARs
Newly-formed
Mature
10,976
7,063
944
579
1935
1254
Total
Gene-TSS
TE-derived
E
DARs (rhEPO vs Placebo)
Newly-formed
Mature
65.2 % (7158)
34.8 % (3818)
66.3 % (4680)
33.7 % (2383)
Percent of Significant DARs
Upregulated
Downregulated
F
Newly-formed
946
4122
5908
Distribution of total DARs (rhEPO vs Placebo)
Proximal promoter (|1| kb from TSS)
Distal promoter (1-10 kb from TSS)
Intergenic and Intronic (> 10 kb from TSS)
G
Newly-formed Neurons
Selected Genes associated with Neurogenesis
Actn1
Ascl1
Bcl11a
Cep95
Dnmt3a
Egr1
Egr2
Egr3
Kalrn
Neto1
Nrg3
Ntrk3
Per2
Ryr1
Septin4
Setd5
Log2 foldchange
rhEPO vs Placebo
Promoter (TSS)
Distance (kb) from TSS DARs (rhEPO vs Placebo)

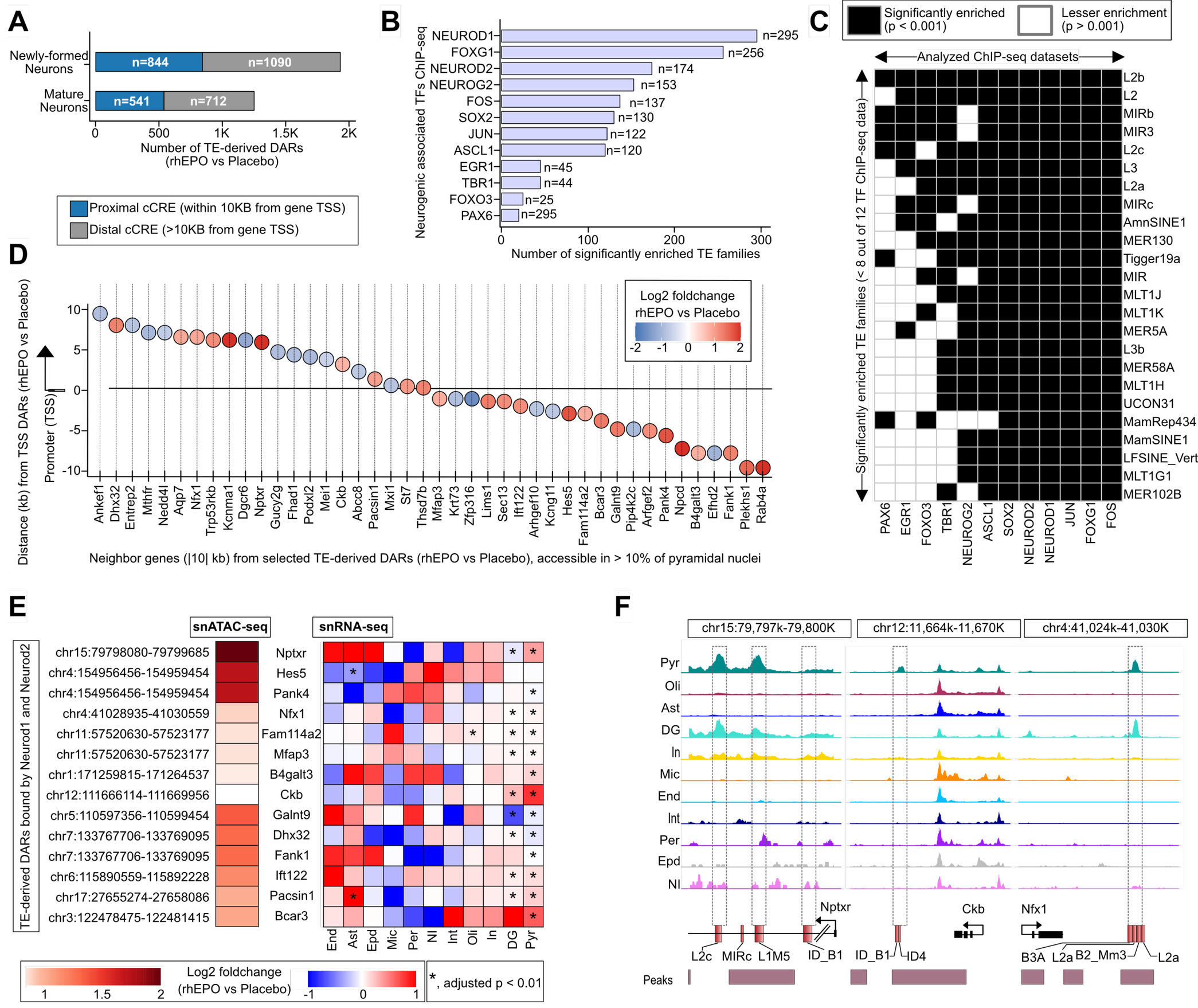
A
Newly-formed Neurons
Mature Neurons
n=844
n=1090
n=541
n=712
0
500
1K
1.5K
2K
Number of TE-derived DARs (rhEPO vs Placebo)
Proximal cCRE (within 10KB from gene TSS)
Distal cCRE (>10KB from gene TSS)
B
Neurogenic associated TFs ChIP-seq
NEUROD1 n=295
FOXG1 n=256
NEUROD2 n=174
NEUROG2 n=153
FOS n=137
SOX2 n=130
JUN n=122
ASCL1 n=120
EGR1 n=45
TBR1 n=44
FOXO3 n=25
PAX6 n=295
0
100
200
300
Number of significantly enriched TE families
C
Significantly enriched (p < 0.001)
Lesser enrichment (p > 0.001)
Analyzed ChIP-seq datasets
Significantly enriched TE families (< 8 out of 12 TF ChIP-seq data)
L2b
L2
MIRb
MIR3
L2c
L3
L2a
MIRc
AmnSINE1
MER130
Tigger19a
MIR
MLT1J
MLT1K
MER5A
L3b
MER58A
MLT1H
UCON31
MamRep434
MamSINE1
LFSINE_Vert
MLT1G1
MER102B
PAX6
EGR1
FOXO3
TBR1
NEUROG2
ASCL1
SOX2
NEUROD2
NEUROD1
JUN
FOXG1
FOS
D
Distance (kb) from TSS DARs (rhEPO vs Placebo)
Promoter (TSS)
10
5
0
-5
-10
Log2 foldchange rhEPO vs Placebo
-2
-1
0
1
2
Ankef1
Dhx32
Entrep2
Mthfr
Nedd4l
Aqp7
Nfx1
Trp53rkb
Kcnma1
Dgcr6
Nptxr
Gucy2g
Fhad1
Podxl2
Mei1
Ckb
Abcc8
Pacsin1
Mxi1
St7
Thsd7b
Mfap3
Krt73
Zfp316
Lims1
Sec13
Ift122
Arhgef10
Kcng11
Hes5
Fam114a2
Bcar3
Galnt9
Pip4k2c
Arfgef2
Pank4
Npcd
B4galt3
Efhd2
Fank1
Plekhs1
Rab4a
Neighbor genes (|10| kb) from selected TE-derived DARs (rhEPO vs Placebo), accessible in > 10% of pyramidal nuclei
E
snATAC-seq
snRNA-seq
TE-derived DARs bound by Neurod1 and Neurod2
chr15:79798080-79799685
chr4:154956456-154959454
chr4:154956456-154959454
chr4:41028935-41030559
chr11:57520630-57523177
chr11:57520630-57523177
chr1:171259815-171264537
chr12:111666114-111669956
chr5:110597356-110599454
chr7:133767706-133769095
chr7:133767706-133769095
chr6:115890559-115892228
chr17:27655274-27658086
chr3:122478475-122481415
Nptxr
Hes5
Pank4
Nfx1
Fam114a2
Mfap3
B4galt3
Ckb
Galnt9
Dhx32
Fank1
Ift122
Pacsin1
Bcar3
End
Ast
Epd
Mic
Per
NI
Int
Oli
In
DG
Pyr
Log2 foldchange (rhEPO vs Placebo)
1
1.5
2
-1
0
1
*, adjusted p < 0.01
F
chr15:79,797k-79,800K
chr12:11,664k-11,670K
chr4:41,024k-41,030K
Pyr
Oli
Ast
DG
In
Mic
End
Int
Per
Epd
NI
Nptxr
Ckb
Nfx1
L2c
MIRc
L1M5
ID_B1
ID_B1
ID4
B3A
L2a
B2_Mm3
L2a
Peaks

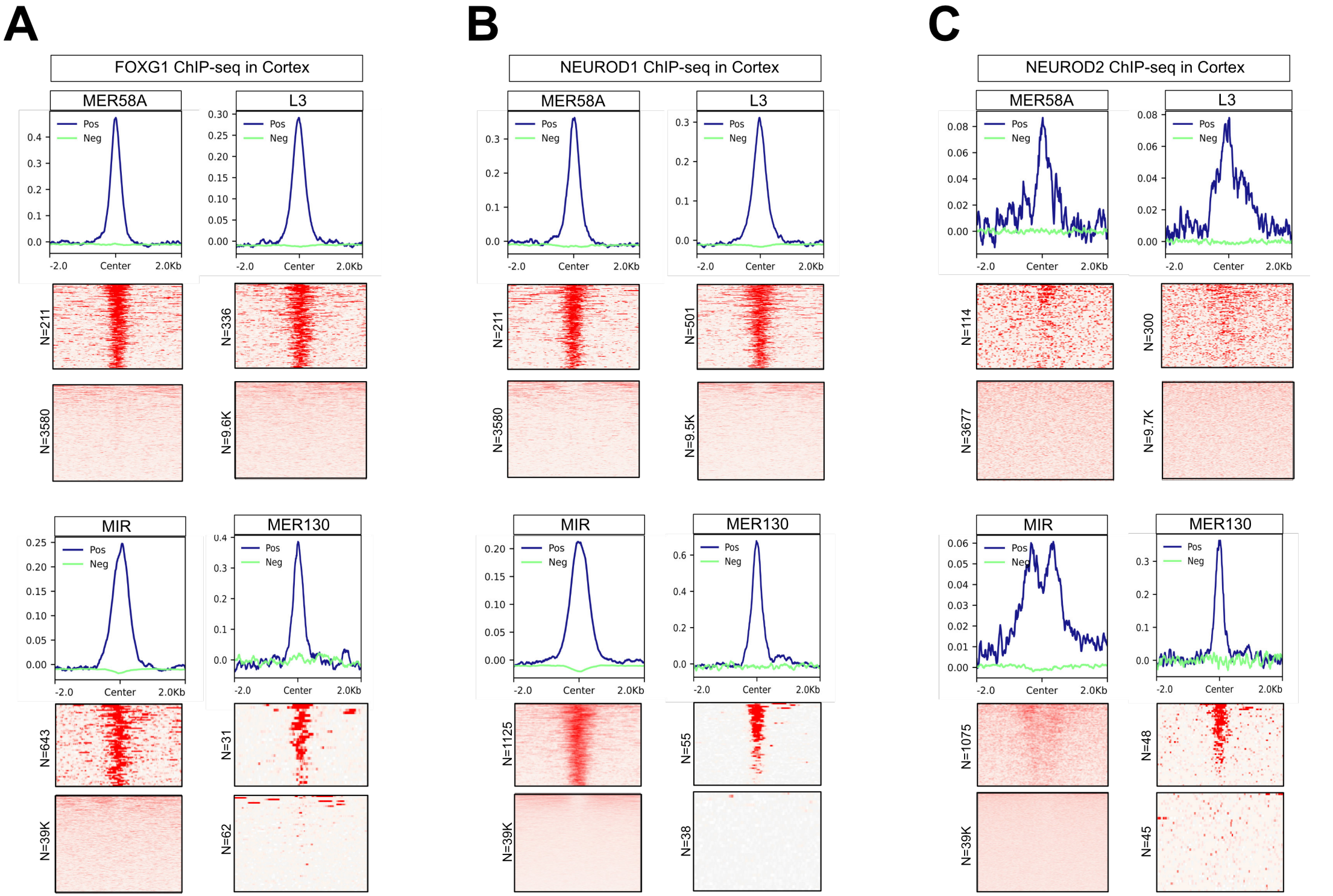
A
FOXG1 ChIP-seq in Cortex
MER58A
L3
MIR
MER130
Pos
Neg
-2.0
Center
2.0Kb
N=211
N=336
N=3580
N=9.6K
N=643
N=31
N=39K
N=62
B
NEUROD1 ChIP-seq in Cortex
N=211
N=501
N=3580
N=9.5K
N=1125
N=55
N=39K
N=38
C
NEUROD2 ChIP-seq in Cortex
N=114
N=300
N=3677
N=9.7K
N=1075
N=48
N=39K
N=45